



## Article

# Hybrid Wind–Redox Flow Battery System for Decarbonizing Off-Grid Mining Operations

Armél Robert, Baby-Jean Robert Mungyeke Bisulandu , Adrian Ilinca \*  and Daniel R. Rousse 

Mechanical Engineering, T3E Research Group, École de Technologie Supérieure (ÉTS),  
Montréal, QC H3C 1K3, Canada; armel.robert.1@ens.etsmtl.ca (A.R.);  
baby-jeanrobert.mungyekobisulandu@etsmtl.ca (B.-J.R.M.B.); daniel.rousse@etsmtl.ca (D.R.R.)

\* Correspondence: adrian.ilinca@etsmtl.ca

## Abstract

Transitioning to sustainable energy systems is crucial for reducing greenhouse gas (GHG) emissions, especially in remote industrial operations where diesel generators remain the dominant power source. This study examines the feasibility of integrating a redox flow battery (RFB) storage system to optimize wind energy utilization at the Raglan mining site in northern Canada, with the goal of reducing diesel dependency, enhancing grid stability, and improving energy security. To evaluate the effectiveness of this hybrid system, a MATLAB R2024b-based simulation model was developed, incorporating wind energy forecasting, load demand analysis, and economic feasibility assessments across multiple storage and wind penetration scenarios. Results indicate that deploying 12 additional E-115 wind turbines combined with a 20 MW/160 MWh redox flow battery system could lead to diesel savings of up to 63.98%, reducing CO<sub>2</sub> emissions by 68,000 tonnes annually. However, the study also highlights a key economic challenge: the high Levelized Cost of Storage (LCOS) of CAD (Canadian dollars) 7831/MWh, which remains a barrier to large-scale implementation. For the scenario with high diesel economy, the LCOS was found to be CAD 6110/MWh, and the corresponding LCOE was CAD 590/MWh. While RFB integration improves system reliability, its economic viability depends on key factors, including reductions in electrolyte costs, advancements in operational efficiency, and supportive policy frameworks. This study presents a comprehensive methodology for evaluating energy storage in off-grid industrial sites and identifies key challenges in scaling up renewable energy adoption for remote mining operations.

**Keywords:** decarbonization; renewable energies; energy storage; redox flow batteries; wind energy; economic analysis



Academic Editors: Konstantinos Braimakis and George Caralis

Received: 25 May 2025

Revised: 18 June 2025

Accepted: 24 June 2025

Published: 25 June 2025

**Citation:** Robert, A.; Mungyeke Bisulandu, B.-J.R.; Ilinca, A.; Rousse, D.R. Hybrid Wind–Redox Flow Battery System for Decarbonizing Off-Grid Mining Operations. *Appl. Sci.* **2025**, *15*, 7147. <https://doi.org/10.3390/app15137147>

**Copyright:** © 2025 by the authors. Licensee MDPI, Basel, Switzerland. This article is an open access article distributed under the terms and conditions of the Creative Commons Attribution (CC BY) license (<https://creativecommons.org/licenses/by/4.0/>).

## 1. Introduction

In the past two decades, dependence on fossil fuels has steadily decreased due to resource depletion and growing concerns over greenhouse gas (GHG) emissions from their combustion. These challenges have prompted governments worldwide to implement strict energy policies to regulate and manage the utilization of both fossil and renewable energy sources. To mitigate GHG emissions, countries that have ratified the Paris Agreement have established regulatory frameworks that set maximum allowable emission thresholds for industries, with penalties for non-compliance. As a signatory to the Paris Agreement, Canada, which accounted for 0.72 Gt CO<sub>2</sub>-equivalent emissions in 2013 (1.95% of global emissions at the time) [1], has committed to reducing national GHG emissions by 40–45% by

2030 and achieving net-zero emissions by 2050 [2–5]. In 2021, the Raglan mine's production process consumed 58.9 million liters of diesel, with electricity generation alone accounting for 73% of this consumption, resulting in 119,440 tons of CO<sub>2</sub>-equivalent emissions. Self-propelled mining equipment accounted for the remaining 27%, emitting 44,400 tons of CO<sub>2</sub> equivalent. To meet these ambitious targets and minimize the environmental and economic risks associated with climate change, transitioning toward decarbonization through the adoption of renewable energy technologies and sustainable energy practices has become imperative [6].

According to Da Silva et al. [7], decarbonization is characterized by three fundamental challenges: (i) replacing fossil fuels with renewable energy sources, (ii) developing alternative solutions for sectors where reducing fossil fuel consumption is particularly difficult, and (iii) eliminating carbon dioxide emissions through advanced mitigation strategies. Du et al. [8] highlight the necessity of a comprehensive transformation in the global electricity sector to achieve effective decarbonization. Similarly, Balaban et al. [9] argue that decarbonizing an energy system requires significant structural changes across the electricity production chain, including generation, transmission, and consumption, as this sector alone accounts for nearly two-thirds of total GHG emissions. Dongsheng et al. [10] further emphasize that ensuring a resilient and sustainable energy future by 2050 is only feasible if power generation integrates cost-effective and scalable renewable solutions. Meanwhile, Obiora et al. [11] and Roshan Kumar et al. [12] stress that a transition to low-carbon energy infrastructures must precede decarbonization efforts, as this remains the most effective approach to reducing the severe environmental impacts of climate change.

Amid the ongoing energy transition, many industrial facilities are actively investing in renewable energy systems to reduce carbon emissions and enhance energy sustainability. In this context, the Raglan mining company in Nunavik, northern Quebec, has committed to decarbonizing its electricity generation network by expanding its wind farm. As a major producer of raw nickel, the site's operations encompass ore exploration, underground excavation, and rock processing, all of which require a reliable and continuous energy supply. Among the most widely adopted renewable alternatives, solar and wind energy are increasingly integrated into off-grid and industrial energy systems. However, due to their intermittent nature and weather dependence, these energy sources require advanced energy storage solutions to ensure grid stability and operational reliability. This study investigates the feasibility of storing surplus wind energy using redox flow batteries (RFBs) to regulate and optimize local electricity production.

For Asri et al. [13], it is, therefore, crucial to critically analyze the fundamental characteristics of energy storage systems (ESSs) in order to establish benchmarks for selecting the most suitable technology. Mahadevan et al. [14] claim that each ESS technology has unique strengths and limitations, influencing its applicability and suitability for specific applications. The choice of an ESS is influenced by factors such as energy density, cost, scalability, and the intended use case, whether for short-term grid balancing or long-term energy storage. It is crucial to consider the climatic conditions of a region before implementing any energy storage system [15]. Table 1 focuses on ESSs currently proficient in providing critical storage capacities of at least 20 MW.

Redox flow battery technology has gained significant attention as a viable solution for large-scale energy storage due to its high efficiency, long cycle life, and independent scalability of power and capacity [16–21]. These batteries are considered one of the most promising technologies for integrating renewable energy into electricity grids [22–24], offering low-cost and long-duration storage capabilities [25]. The large-scale deployment of variable renewable energy resources is heavily influenced by the availability of cost-effective, long-duration storage solutions [26]. Despite their advantages, flow batteries

accounted for only 5% of the 16 GWh installed energy storage capacity worldwide in 2021, highlighting the need for further technological advancements and economic optimizations to expand their adoption.

**Table 1.** Comparison and characteristics of energy storage systems [13].

Storage System Type	Max Power Rating [MW]	Discharge Time	Max Cycles or Lifetime	Energy Density [Wh/L]	Efficiency
Pumped hydro	~3000+	4 h–16 h	30–60 years	0.2–2	70–85%
Compressed air	~1000	2 h–30 h	20–40 years	2–6	40–70%
Molten salt	100–150	Several hours	~30 years	70–210	80–90%
Li-ion battery	1–100+	1 min–8 h	1000–10,000 cycles	200–400	85–95%
Lead–acid	1–100	1 min–8 h	6–40 years	50–80	80–90%
Flow battery	10–100+	Several hours	12,000–14,000 cycles	20–70	60–85%
Hydrogen	~100+	Minutes–weeks	5–30 years	~600 (at 700 bar)	25–45%
Flywheel	1–20	Seconds–minutes	20,000–100,000+ cycles	20–80	70–95%

A flow battery is a reversible and rechargeable electrochemical system that stores energy in chemical form and converts it back into electrical energy when needed. The fundamental operating principle of these batteries involves the circulation of an electrolytic solution (electrolyte) from one or more storage reservoirs into electrochemical cells facilitated by pumps [16,27]. These cells, consisting of two half-cells (positive and negative), serve as the site for redox reactions, enabling the storage and release of energy. Flow batteries can be configured in series and/or parallel to achieve the desired voltage and current characteristics. They are often considered a hybrid technology between fuel cells and conventional batteries, where hydrogen ( $H_2$ ) and oxygen ( $O_2$ ) gases in fuel cells are replaced by electrolytes capable of storing electrical charges [28]. The schematic representation of a flow battery system is illustrated in Figure 1.

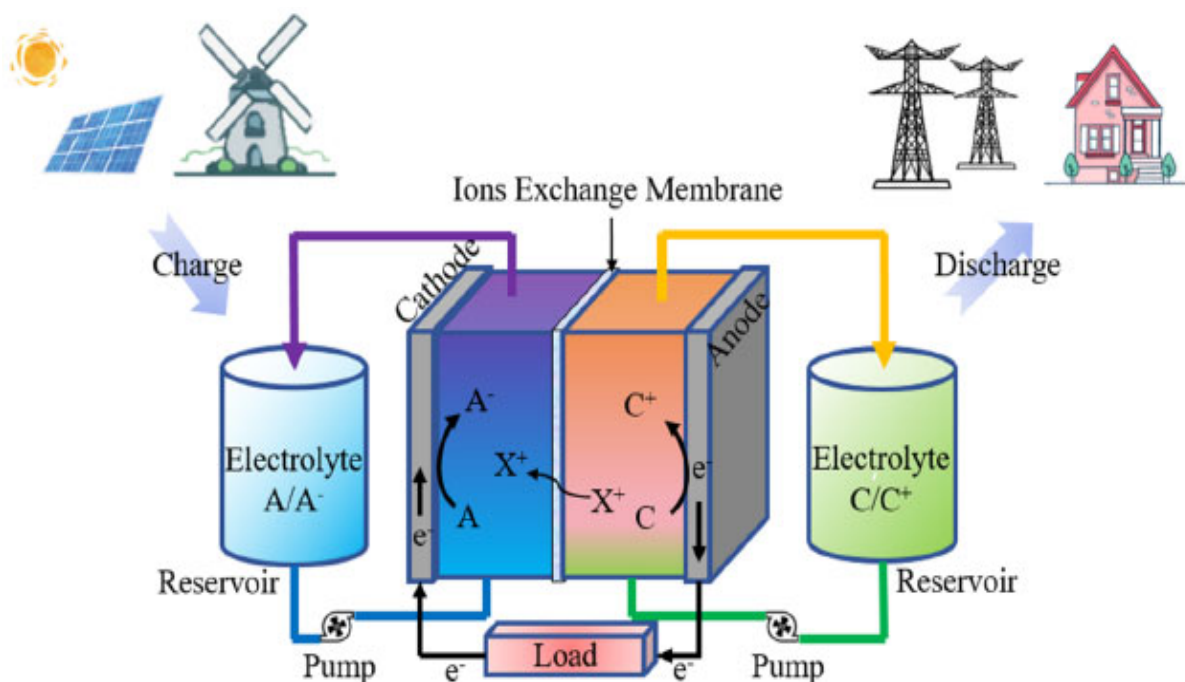


**Figure 1.** Schematics and working principle of redox flow batteries [16].

Several studies have explored the application of flow batteries for energy storage in different renewable energy systems. Ouyang et al. [25] investigated the performance of a vanadium redox flow battery (VRFB) within a microgrid integrating a biomass gasifier and a solid oxide fuel cell designed for electricity generation in rural environments (Figure 2). Their findings indicate that the electrolyte flow rate plays a crucial role in battery performance, with an efficiency of 84% achieved during peak shaving operations.

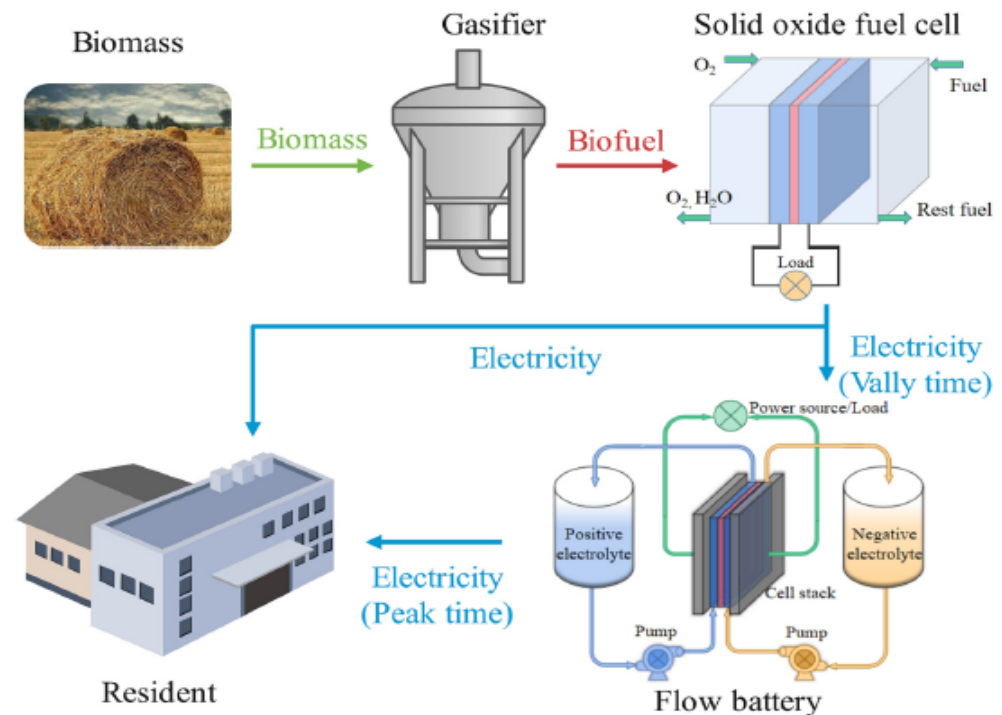


**Figure 2.** Flow battery in a renewable energy microgrid [25].

Zheng et al. [29] examined the integration of a flow battery system to address the intermittency of renewable energy sources while managing fluctuating energy demand. The proposed energy system featured a hybrid setup comprising a partially covered parabolic mirror thermal photovoltaic collector, a vanadium redox flow battery, thermal energy storage, and an absorption chiller/heat pump. Their comparative analysis between a VRFB-based system and a Power-to-Hydrogen-to-Power (P2H2P) system revealed that the VRFB system achieved an exergy efficiency of 78.52%, outperforming the P2H2P system, which had an efficiency of 41.73%.

Yesilyurt et al. [30] explored the feasibility of powering an air-source hybrid heat pump using a vanadium redox flow battery-based energy storage system. Their study selected two key performance indicators: exergy destruction and exergy efficiency. Using a MATLAB Simulink model, they analyzed a system where solar photovoltaic panels and wind turbines charged the VRFB. The results showed that integrating wind turbines with the VRFB was more effective, as the photovoltaic-based system exhibited significant exergy destruction and lower exergy efficiency.

In a different study, Oshnoei et al. [31] presented a load frequency control model for a wind power system and redox flow battery storage. Their findings demonstrated that frequency-based VRFB modeling yielded superior performance compared to conventional VRFB modeling techniques, highlighting the potential of flow batteries in enhancing grid stability.

Among the different types of flow batteries, all-vanadium redox flow batteries (VRFBs) stand out due to their flexibility, adaptability, and scalability. Reynard and Girault [32]

investigated redox flow battery technology for energy storage and clean hydrogen production, integrating VRFBs with catalytic reactors to enhance efficiency. Huang et al. [33] estimated the overall efficiency of such systems to range between 70% and 85%, while Ulaganathan et al. [34] reported efficiencies exceeding 83%, a value often used as a benchmark for sizing battery systems.

One key advantage of all-vanadium flow batteries is their ability to independently scale storage capacity and power output. Hosseiny and Wessling [35] and Skyllas-Kazacos et al. [36] emphasize that increasing storage capacity is directly proportional to the electrolyte volume, necessitating larger electrolyte reservoirs for extended operation. Zhang et al. [36] further highlight that increasing the battery's storage capacity and cycle duration can effectively reduce capital expenditure (CAPEX) per kilowatt-hour, improving the economic feasibility of large-scale deployments.

The economic viability and resilience of hybrid energy system solutions depend on a comprehensive evaluation of economic and reliability factors during the design phase [37]. In the literature, numerous studies have investigated the investment costs and financial feasibility of redox flow battery (RFB) storage systems for large-scale energy applications. Cremoncini et al. [38] classify two primary approaches to the techno-economic analysis of RFBs: The first focuses on material and investment costs. In contrast, the second incorporates Levelized Cost of Storage (LCOS) models to assess long-term financial sustainability. Darling [26] conducted a detailed techno-economic study on redox flow batteries, demonstrating that capital and operational costs, combined with projected energy throughput, are key determinants of LCOS.

According to IRENA [39], the costs of vanadium and zinc/bromine flow batteries could decline by more than 60% over the next two decades, driven by technological advancements and growing market interest. Similarly, Schmidt et al. [40] predict a steady reduction in redox flow battery costs due to economies of scale and material innovations. Minke and Turek [41] emphasize that assessing the techno-economic feasibility of RFBs remains a significant challenge for large-scale projects, where system costs must be evaluated based on material composition, system design, and modeling methodologies.

Zheng et al. [42] emphasize the need for a deeper understanding of the technical and economic performance parameters of flow battery technologies to enhance their commercial viability. Zhang et al. [43] further highlight that cost challenges remain a significant barrier to the widespread adoption of RFBs. Noack et al. [44] advocate for optimization strategies in vanadium redox flow battery systems, particularly in reducing material costs, optimizing bipolar plate resistances, and improving energy storage media efficiency.

To support cost reductions, Viswanathan et al. [45] developed a cost model for redox flow batteries, revealing that the energy-to-power ratio of the storage system is a crucial factor in minimizing costs across various battery chemistries. Additionally, LCOE reductions are influenced by integrating advanced materials (e.g., novel alloys), improved manufacturing processes, and higher nominal power capacities [46]. Currently, the levelized cost of energy (LCOE) for redox flow batteries is estimated at CAD 0.0503/kWh [29]. Ouyang et al. [25] report a payback period of 7.33 years for a microgrid equipped with a vanadium redox flow battery, further reinforcing the economic feasibility of this technology. In the literature, LCOS models for redox flow batteries have been widely utilized to evaluate cost-effectiveness across different storage applications [38,40].

This study evaluates the feasibility of integrating a redox flow battery storage system with an expanded wind farm at the Raglan mining site. This research utilizes a MATLAB R2024b-based simulation model to evaluate the technical, economic, and environmental impacts, with a focus on diesel savings, CO<sub>2</sub> emissions reduction, and system reliability. Unlike previous studies focusing on standalone storage systems, this research integrates



a comprehensive techno-economic analysis, comparing multiple wind–battery hybrid scenarios. Specifically, it examines how different battery capacities (80 MWh, 120 MWh, 160 MWh) and wind penetration levels (45–75%) affect the Levelized Cost of Energy (LCOE) and Levelized Cost of Storage (LCOS), key determinants of project feasibility [26,44].

The key research questions guiding this study are as follows:

1. What is the optimal configuration of wind energy and redox flow storage to maximize diesel savings at the Raglan mining site?
2. What are the economic implications of integrating large-scale redox flow batteries, particularly in Arctic conditions?
3. How does energy storage improve grid stability, and what policy incentives could enhance financial feasibility?

This article is part of a broader research initiative exploring various energy storage technologies to support the decarbonization of remote mining operations in northern Quebec. In addition to the redox flow battery system analyzed in this study, parallel investigations are underway on battery energy storage systems (BESS), hydrogen storage, and PHSP systems [47,48]. These complementary studies evaluate each option based on technical performance, economic viability, and environmental compatibility within off-grid Arctic contexts. However, due to the ongoing comparative analysis, this paper focuses solely on the techno-economic feasibility of implementing a redox flow battery system in the Raglan hybrid electricity network.

Building on this context, the present work investigates the potential for significantly reducing or even eliminating diesel dependency at the Raglan mine by integrating a wind farm coupled with a redox flow battery storage system. Specifically, it examines how this hybrid “Diesel Thermal Power Plants–Wind Farm–redox battery” configuration can address the intermittency of wind energy and maintain a stable electricity supply across the mine’s 25 kV-G network. The study involves the overall dimensioning of the wind–redox battery system, assessing its ability to meet electricity and heating demands, and techno-economic feasibility analysis to support future investment and implementation decisions.

The findings of this study offer valuable insights for industrial energy planners, policymakers, and renewable energy developers, providing a scalable model for integrating storage systems in off-grid mining operations.

Given that this work focuses on decarbonizing the Raglan mine through the sizing and optimization of a hybrid energy system based on redox flow battery storage, the model aims to minimize the levelized cost of electricity (LCOE) while maximizing system performance. Accordingly, the outputs of the optimization process include

- Economic indicators: capital and operating expenditures, energy price, payback period, and net present value (NPV);
- Technical indicators: installed capacity and power, number of wind turbines, wind penetration rate, number of generators in operation or removed, redox battery capacity, and greenhouse gas (GHG) emission reduction.

The specific objective of this work is to study the feasibility of integrating a redox flow battery (RFB) storage system into the Raglan mine site’s hybrid grid to reduce diesel dependence, improve grid stability, and enhance energy security (optimizing wind farm energy production and addressing wind farm intermittency).

Table 2 summarizes relevant work on RFB applications.

**Table 2.** Summary of works applying RFB technology.

References	Context-Application	Storage System	Results
Zheng et al. [29]	To address the intermittency of renewable energy sources To manage fluctuating energy demand	VRFB system	Exergy efficiency of 78.52%
Yesilyurt et al. [30]	Powering a hybrid air-source heat pump	VRFB system	Efficiency of wind turbine integration with VRFB
Oshnoei et al. [31]	Load frequency control model for a wind power system	VRFB system	Higher performance due to the use of frequency-based VRFB
Reynard and Girault [32]	Energy storage Clean hydrogen production, integrating VRFBs with catalytic reactors to enhance efficiency	VRFB system	Improving the efficiency of catalytic reactors
Ouyang et al. [25]	Performance of a VRFB within a microgrid integrating a biomass gasifier and a solid oxide fuel cell designed for electricity generation in rural environments	VRFB system	Battery performance is highly dependent on the flow of the electrolyte. An efficiency of 84% was achieved during peak shaving operations.

The rest of this paper is organized as follows: Section 2 briefly describes the energy system; Sections 3 and 4 detail the methodology, including the design and sizing of the wind energy storage system, as well as the assumptions and modeling framework used to assess the technical, economic, and environmental feasibility of integrating redox flow batteries (RFBs); Section 5 presents the validation of the model with global data at Raglan mine; Section 6 discusses the results, including economic feasibility and grid performance; and Section 7 outlines the conclusions and recommendations for future energy storage projects.

## 2. System Description

The Raglan mining site, located in northern Quebec, Canada, operates a localized energy network known as “Network 25 kV-G,” which supplies both electricity and heat to the site. This network comprises twenty diesel generators and a wind farm with two operational wind turbines. Among these twenty generators, six EMD models (see Figure 3) are equipped with heat recovery loops, forming a cogeneration system that meets the site’s thermal energy demands.

As part of its decarbonization strategy, the Raglan mining company is committed to reducing diesel consumption, a major contributor to the site’s greenhouse gas (GHG) emissions. Given the high wind energy potential in the region, the company plans to expand the existing wind farm by adding additional wind turbines to replace the diesel generators scheduled for decommissioning. However, due to the intermittent nature of wind energy, integrating an energy storage solution is essential to ensure grid stability, reliability, and continuous energy supply. To address these challenges, the company is considering a redox flow battery (RFB) storage system to help mitigate wind energy fluctuations and regulate the 25 kV-G network during peak and low-demand periods.

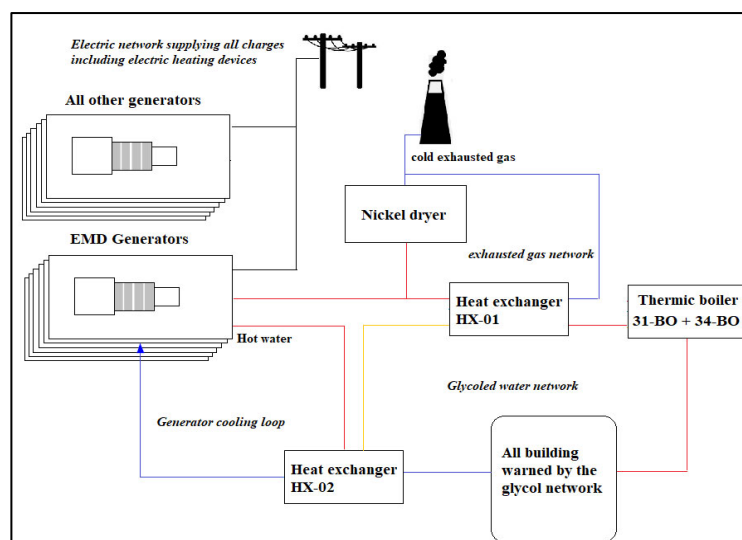


Figure 3. Scheme of the electrical and heating networks.

The VRB ENERGY all-vanadium redox flow battery, manufactured by a Vancouver-based Canadian company, has been selected for this application (see Figure 4). This battery technology offers high efficiency, long cycle life, and independent scalability of power and capacity, making it well-suited for large-scale renewable energy storage at the Raglan site.

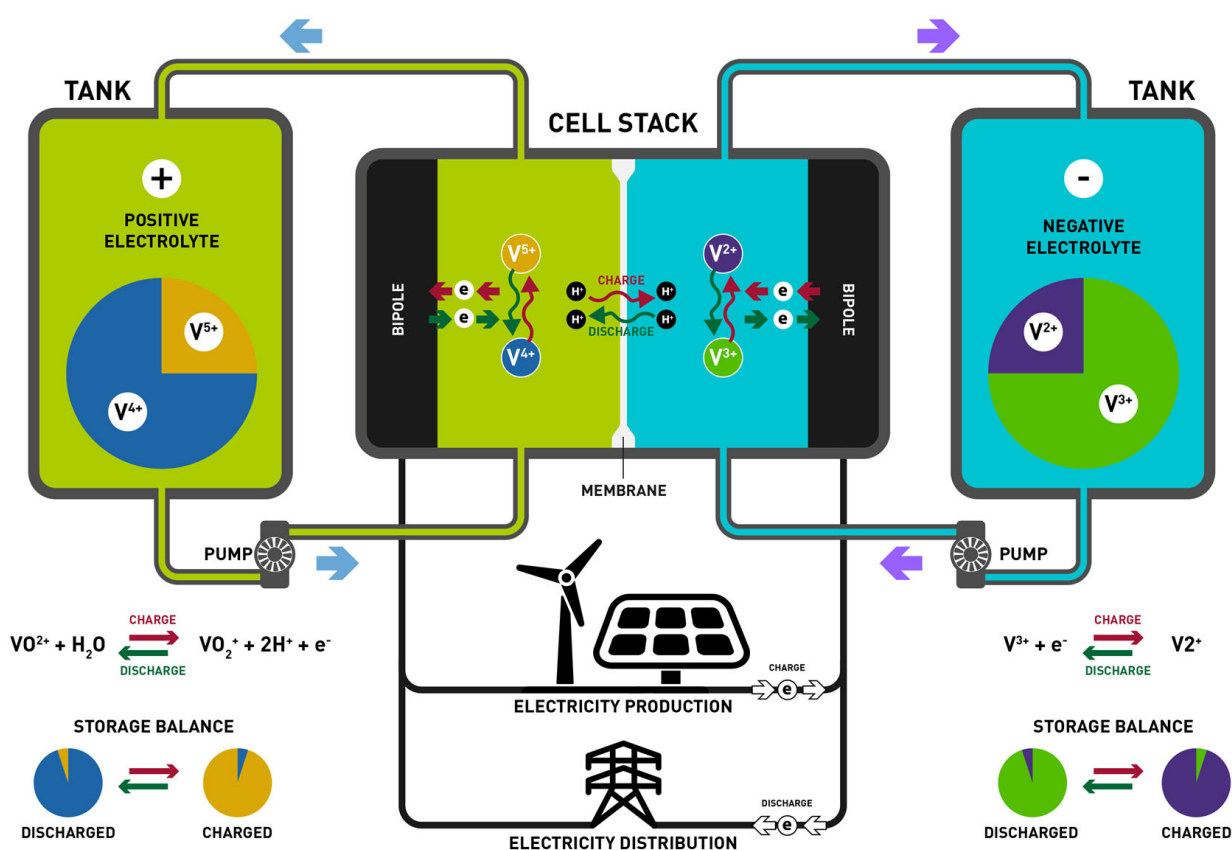


Figure 4. VRB ENERGY all-vanadium flow battery: battery model VRB-ESS, 1 MW, 500 MWh of energy storage capacity installed or in development [49].

The project's first phase focuses on optimizing wind farm production, ensuring a complete transition from diesel generators, meeting electrical and thermal energy demands, and appropriately sizing the redox flow battery required for the site's operations. The



successful implementation of this hybrid wind–storage system plays a critical role in achieving the site’s long-term energy transition and sustainability goals.

### 3. Methodology

This study aims to design and optimize a wind energy storage system utilizing redox flow batteries (RFBs) at the Raglan mining site, thereby reducing diesel consumption and decarbonizing electricity production. The MATLAB-based simulation model developed for this study integrates wind power generation, battery storage dynamics, load demand, and economic feasibility analysis. The main equations used in the model are presented in Appendix A.

#### 3.1. Assumptions

The simulation is based on the 2020 operational data from the Raglan site, considering the following key assumptions:

- Energy demand: The mine’s annual electricity consumption is 145,195 MWh, requiring 34.2 million liters of diesel. The daily average electricity consumption of the site is shown in Figure 5.

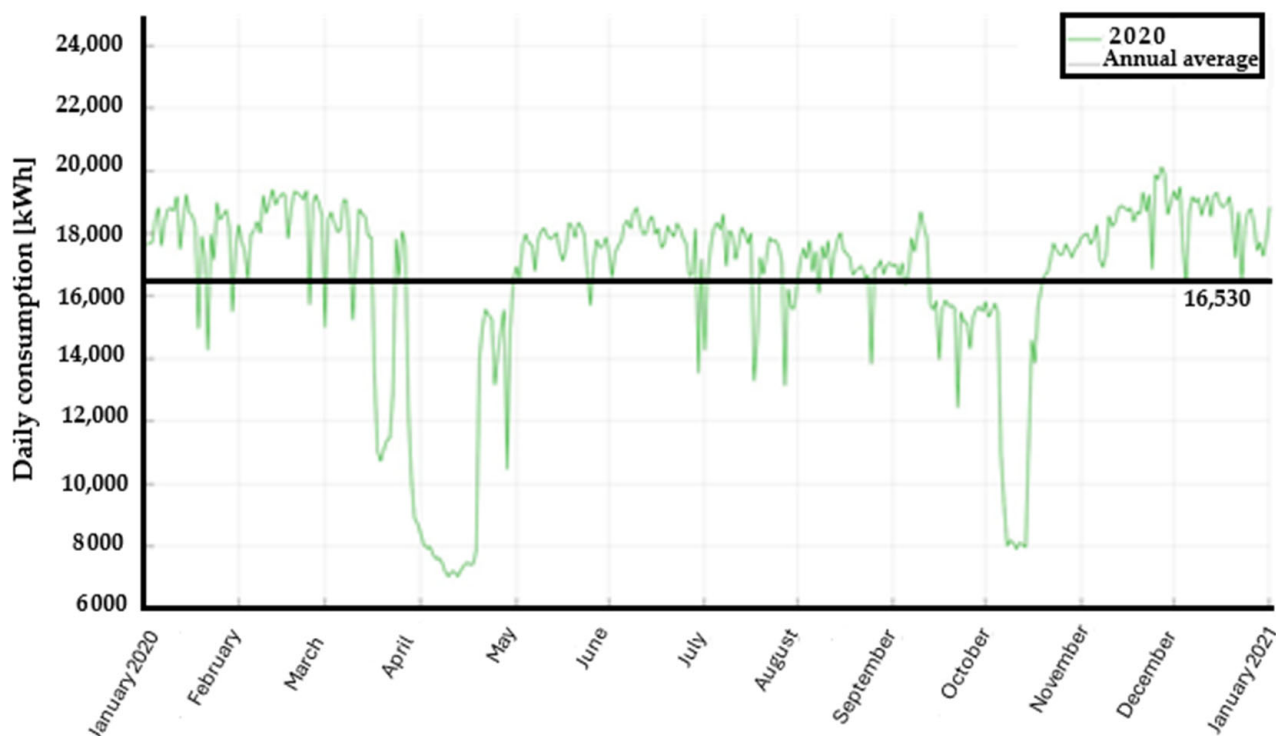


**Figure 5.** Daily electricity consumption of the 25 kV network in 2020.

- Wind resource: Wind speed data from 2020 indicates monthly average speeds between 6 and 9 m/s (see Figure 6) with an annual average of 8.5 m/s at the wind turbine hub height (92 m).
- Ambient temperature: The average temperature on site is  $-15^{\circ}\text{C}$ , which affects air density ( $1.367\text{ kg/m}^3$  instead of the standard  $1.225\text{ kg/m}^3$ ).
- Wind farm expansion: The existing two wind turbines (Enercon E-82) are expected to be supplemented with newer E-115 EP3 E4 turbines, each with a rated power of 4260 kW (92 m hub height) and a power curve illustrated in Figure 7.
- Battery storage: The selected VRB ENERGY all-vanadium flow battery is installed in a heated facility to mitigate cold-related efficiency losses.

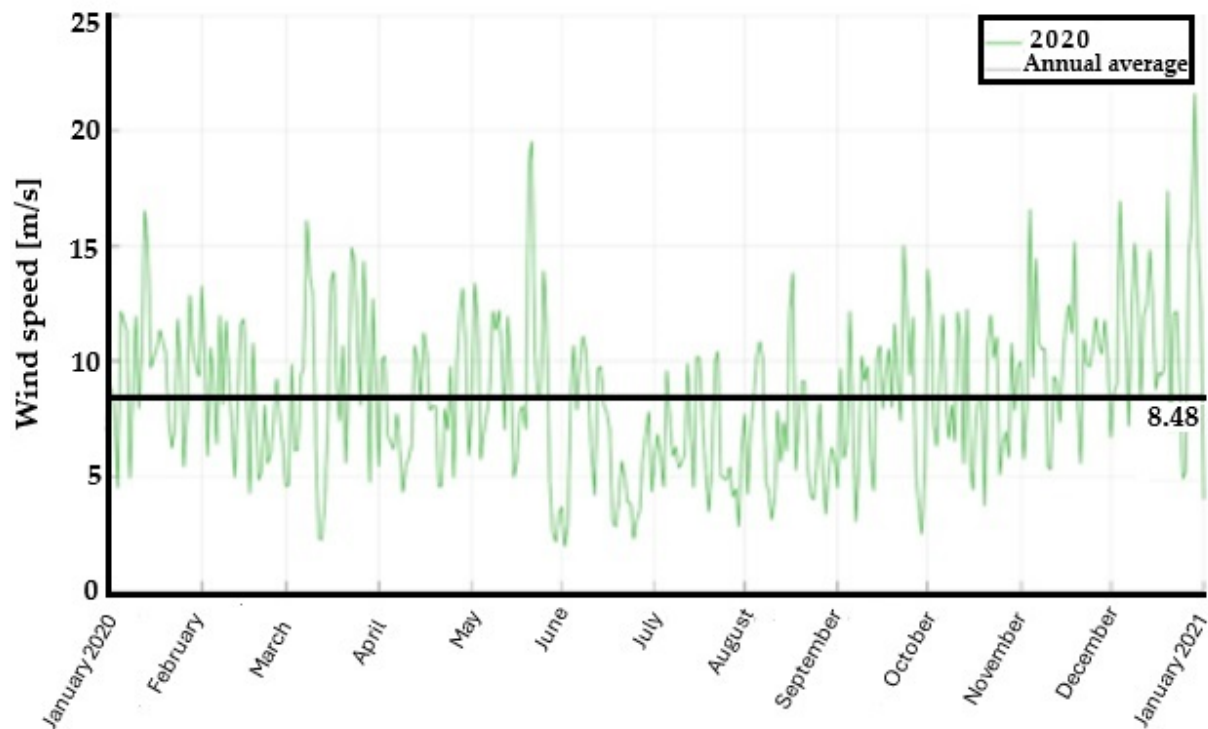


Figure 6. Wind speed in 2020 in Raglan.

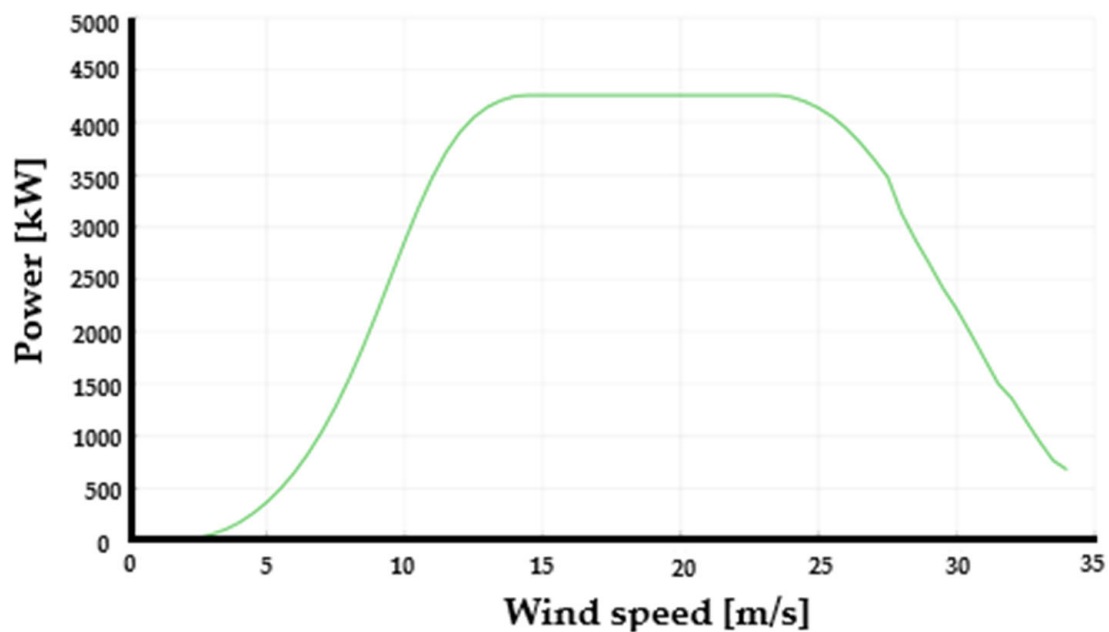
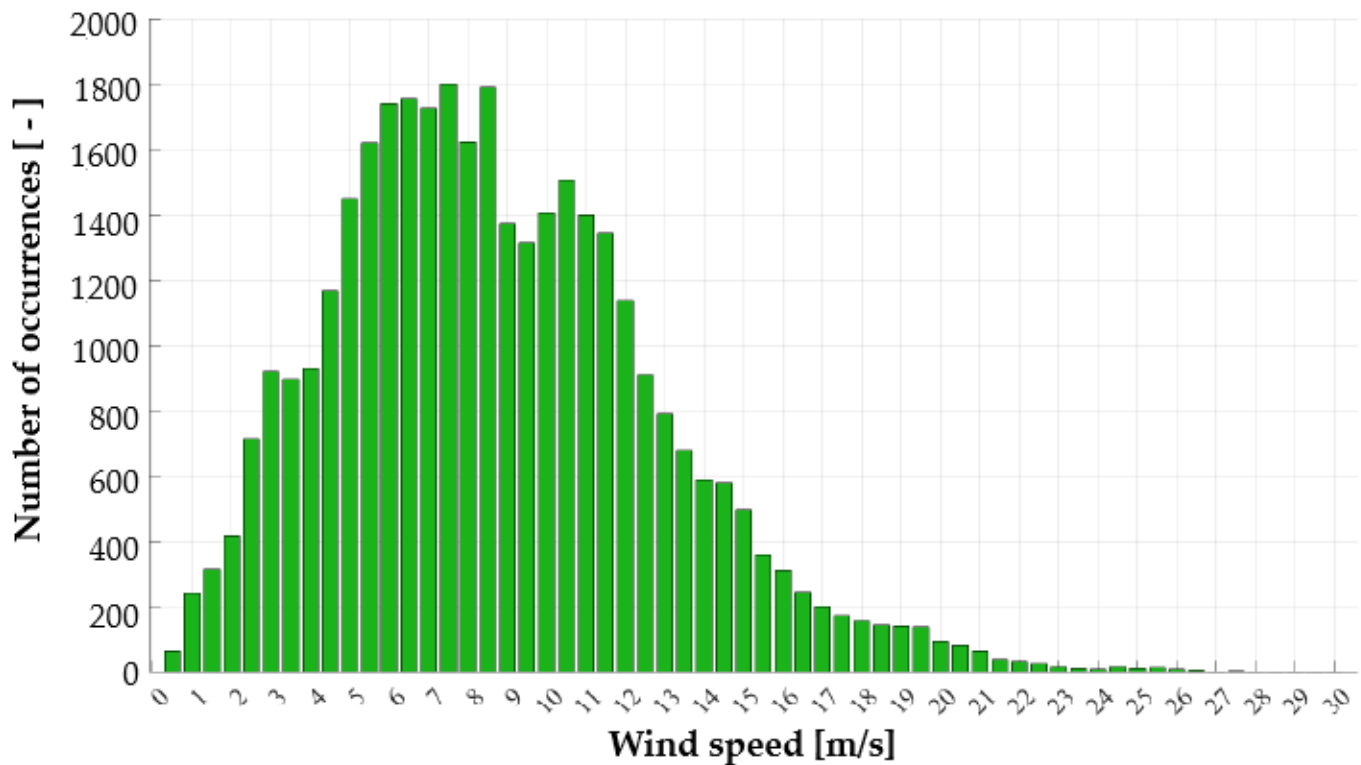


Figure 7. The power curve of the E-115 EP3 E4 wind turbine.

### 3.2. Wind Energy Production in Mining Sites: Forecasting, Optimization, and Utilization

Given that wind production is highly dependent on wind speed, this study used wind speed data from several years (2017–2018–2019–2020–2021). The year 2020 was chosen as it was the most representative compared with the other years. An average speed of approximately 8.5 m/s was therefore established over the year. This is homogeneous. Figure 8 shows the occurrence of wind speeds at quarter-hourly intervals over the year 2020.



**Figure 8.** Frequency of occurrence of different wind speeds in 2020.

The distribution of Figure 8 is made possible using Equation (A5) in Appendix A.

From the wind data (wind potential of the site) of the Raglan mining site, the power available for each of the wind turbines is deduced using the information provided by the manufacturer. For example, the E-115 EP3 E4 wind turbine (Enercon, Aurich, Germany) produces 3472 MW, while the E-82 E4 wind turbine (Enercon, Aurich, Germany) produces 1880 MW when the wind speed reaches 11 m/s. As wind speeds are dependent on the seasons and the weather, energy production from wind turbines is also dependent on them. Except for violent winds (storms, etc.) with speeds of up to 26.5 m/s, wind production is higher when the wind is stronger. Thus, the wind distribution at the Raglan site follows a Weibull distribution, and its shape is characteristic of it (see Figure 8).

Considering that wind energy production is intermittent, the project plans to couple the wind farm with a redox flow battery storage system.

To study the periods without wind at Raglan, an assumption is made that considers a wind speed of less than 3 m/s to be a period without wind. This assumption is based on the fact that the E-115 wind turbine does not produce even 80 kW below 3 m/s, which is required for de-icing. In 2020, there was 643 h without wind over the whole year. The longest period without wind was 28 consecutive hours. During this 643 h, almost 100% of electricity production would have to rely on diesel generators (see Figure 9).

The periods without wind, representing more than 61% of cases, are shorter than eight hours. This indicator can be used to determine the battery size and its storage life.

### 3.3. Sizing of the Energy System

Raglan mine is set to expand its renewable energy capacity by 2030, with wind energy selected as the primary source due to the region's abundant wind resources and the success of its initial wind turbine project, which currently operates two turbines. The additional wind energy generated should be integrated into the 25 kV-G network, marking a significant milestone in the site's decarbonization efforts. This transition reduces reliance

on diesel generators, enhances energy sustainability, and aligns with broader carbon reduction targets.

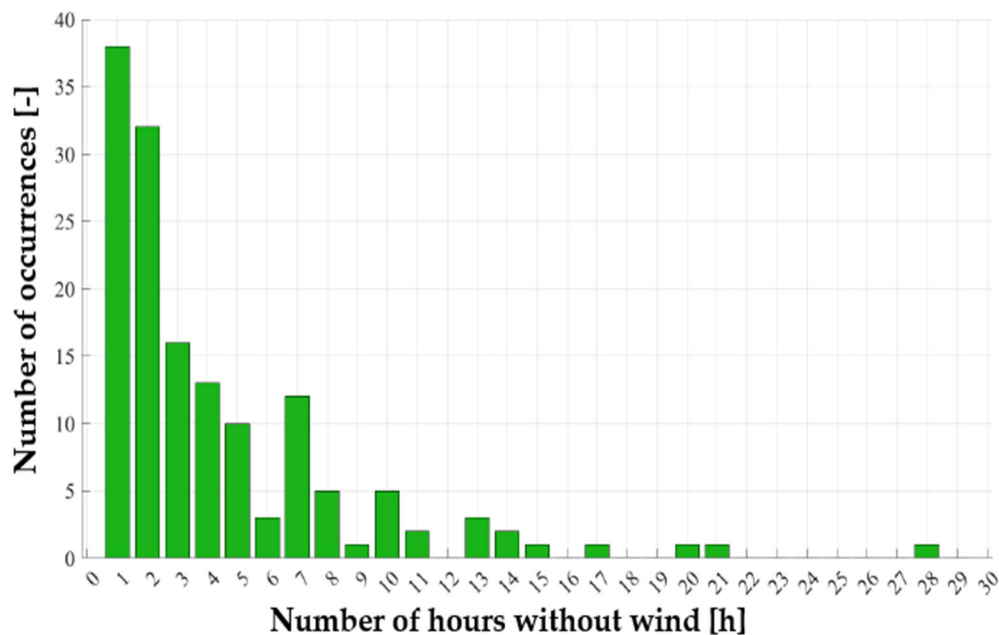


**Figure 9.** Number of occurrences of windless periods.

### 3.3.1. Sizing, Installation, and Cost of the Wind Farm

Proper sizing and installation of the wind farm are critical, as site-specific characteristics directly influence turbine performance. The Raglan mining site in northern Canada experiences extreme cold temperatures throughout the year, making wind energy more suitable than solar power due to limited sunlight availability. Among the various renewable energy sources, wind power is particularly well-adapted to the climatic conditions of northern Canada [48].

As mentioned, the Raglan site currently operates two Enercon E-82 E4 wind turbines, each with a nominal power output of 3 MW, integrated into the 25 kV grid network. To expand the site's renewable energy capacity and advance its decarbonization objectives, the current project proposes deploying additional wind turbines of the latest ENERCON model, the E-115 EP3 E4. This upgraded model, featuring a 92 m mast and a nominal power rating of 4.260 MW, represents a 42% increase in capacity compared to the existing turbines. Table 3 summarizes the key characteristics of the wind turbines at the Raglan mine site.

**Table 3.** Characteristics of the wind turbines at the Raglan mine site.

Types of Wind Turbine	Minimum Wind Speed for a Wind Turbine Operation	Wind Speed to Reach Maximum Power	Maximum Operating Wind Speed of the Wind Turbine
E-82	3 m/s	17 m/s	26 m/s
E-115	2 m/s	14.5 m/s	34 m/s

The E-115 wind turbine is significantly larger than its predecessor, featuring a rotor diameter of 115.7 m and a sweep area of approximately 10,516 m<sup>2</sup>. One of its key advantages is the ability to generate higher energy output while reducing the number of turbines required, thereby minimizing land use and environmental impact. Additionally, this model

is specifically designed to withstand Arctic conditions, including frost, extreme cold, and severe storms. Given the site's environmental challenges, the estimated operational lifespan of the wind turbines is conservatively set at 15 years for design purposes. However, the manufacturer specifies a lifespan of 25 years under standard operating conditions.

Due to the extensive size of the Raglan mining site, careful selection of the wind farm's location is essential to ensure optimal connectivity to the 25 kV-G electrical network while facilitating access for maintenance teams. The area surrounding Katinniġ has been identified as the most suitable location for the additional wind turbines. LiDAR (Light Detection and Ranging) studies are planned to further refine site selection and optimize turbine placement, enabling the accurate assessment of wind characteristics, including speed, intensity, and directional patterns.

A thorough analysis of investment costs is crucial in large-scale projects, as it informs key decisions regarding equipment selection, financial feasibility, and trade-offs between technical performance and site-specific constraints. Understanding these costs is essential for optimizing project design while balancing economic and environmental considerations.

In recent years, the cost of wind energy projects has significantly declined and is expected to continue decreasing in the coming decades. According to Stehly and Duffy [50], this trend is driven by improvements in turbine performance, reduced energy losses and operational risks, enhanced cost management, and advances in materials and construction techniques.

To evaluate the financial feasibility of the wind energy expansion at Raglan, this study employs the Levelized Cost of Energy (LCOE) metric. LCOE is a key economic indicator that provides a comparative assessment of different energy technologies. It consists of two main components: capital expenditure (CAPEX), which represents upfront investment costs, and operating expenditure (OPEX), which includes maintenance and operational expenses. LCOE is typically expressed in CAD/kWh or CAD/MWh and is influenced by five primary factors: initial capital investment, ongoing operational costs, system performance, financial and tax assumptions, and project lifespan.

The study also incorporates data from the IRENA report [46], which provides relevant insights specific to Canada, including the Raglan mining site. Based on these indicators and the referenced report, the cost analysis yielded the results in Table 4.

**Table 4.** Wind CAPEX, OPEX, and LCOE in Canada and Raglan.

Localization	OPEX (CAD/kW·yr)	OPEX (CAD/MWh)	CAPEX (CAD/kW)	CAPEX (CAD/MWh)	LCOE (CAD/MWh)
Canada	46.9	11.84	1833	23.15	35.0
Raglan	117.6	30.76	4857	84.69	115.5

The results indicate a substantial increase in both OPEX (150.8%) and CAPEX (164.9%) for the Raglan site compared to the national average, primarily due to the site's extreme environmental conditions, including harsh winters and remote location.

The price of an ENERCON E-115 EP3 E4 wind turbine (4.260 MW) for the Raglan site is calculated at approximately CAD 20,690,000 using the cost estimates from Table 4. A simplifying assumption was adopted to determine the total wind farm investment cost, wherein the cost of a single wind turbine is multiplied by the total number of turbines planned for deployment.

### 3.3.2. Sizing, Implementation, and Cost of the Storage System

Despite the abundant wind energy potential at the Raglan site, an energy storage solution is essential to mitigate wind power's intermittency and ensure grid stability.



This study assesses the feasibility of integrating redox flow batteries (RFBs) as the primary storage technology, given their proven advantages, pre-installation readiness, and technological maturity.

To accurately size the storage system for the Raglan mining site, this study relies on agency reports, laboratory data, and direct manufacturer specifications. Given the region's extreme climatic conditions, a critical design consideration is protecting batteries from subzero temperatures. While redox flow battery systems are typically delivered in insulated containers, prolonged exposure to temperatures below  $-5\text{ }^{\circ}\text{C}$  can cause performance degradation. Specifically, low temperatures can impair electrolyte flow, reduce electrochemical efficiency, and shorten system lifespan. To mitigate these risks, the storage units are housed in a heated shed, ensuring protection against snow, wind, and frost while maintaining optimal operating conditions.

Two key parameters determine the size of the shed:

- The footprint of the redox battery system;
- The required storage capacity.

This study directly consulted battery manufacturers since literature sources do not provide standard values for redox battery footprints. The responses varied between  $30\text{ m}^2/\text{MWh}$  and  $80\text{ m}^2/\text{MWh}$ , with an average value of  $50\text{ m}^2/\text{MWh}$  selected for this project. Given the large footprint of the mining site, the battery storage facility is strategically located near the main complex in Katinni, ensuring efficient integration into the mine's energy circuit.

As with the wind farm investment analysis, the cost estimation for redox batteries is a critical aspect of the feasibility assessment. Due to the harsh environmental conditions at Raglan, cost adaptations are necessary to account for additional infrastructure requirements. This study uses the Levelized Cost of Storage (LCOS) metric to quantify the financial viability of storage deployment.

LCOS represents the cost per kWh of stored electricity over the system's lifetime, incorporating capital (CAPEX) and operational (OPEX) expenses. This metric provides a long-term perspective on the economic feasibility of storage solutions, where a lower LCOS indicates greater profitability [51]. Table 5 presents the estimated LCOS for the Raglan site based on different storage durations.

**Table 5.** LCOS of redox systems at Raglan (CAD/MWh).

Parameters	10 MW, Raglan		
	4 h	6 h	8 h
<b>Storage system</b>			
Storage unit and electrolyte	118.1	105.2	98.3
Storage balance	23.6	21.0	19.8
<b>Energy system</b>			
Power supply equipment	14.3	9.5	7.1
Control and communication	0.9	0.6	0.4
System Integration	21.9	19.3	18.0
<b>System balance</b>			
Engineering, transportation, and construction	83.0	73.0	68.7
Project development	41.8	37.2	34.9

**Table 5.** *Cont.*

Parameters	10 MW, Raglan		
	4 h	6 h	8 h
Network Integration	9.0	6.0	4.5
Total CAPEX	312.5	271.8	251.8
Total OPEX	35.3	33.9	33.3
Total LCOS	347.8	305.8	285.0

The estimated LCOS values of 347.8, 305.8, and 285.0 CAD/MWh correspond to 4 h, 6 h, and 8 h storage durations, respectively. These values align with literature estimates and manufacturer-provided data, confirming their validity as benchmarks for cost assessment. Note here that LCOS also represents the total lifetime cost of the storage system (including operating and maintenance costs), divided by the total amount of electricity that the system is expected to store during its lifetime [51]. Based on the above cost assessments, Table 6 presents the final investment costs for the redox battery system and associated infrastructure, specifically for a 20 MW system at Raglan.

**Table 6.** Final costs of redox batteries.

Parameters	20 MW, Raglan		
	4 h	6 h	8 h
<b>Electrochemical system (M CAD)</b>	117.0	152.7	188.6
<b>Area required (m<sup>2</sup>)</b>	4000	6000	8000
<b>Shed price (M CAD)</b>	32.5	48.8	65.0
<b>Total cost (M CAD)</b>	149.5	201.4	253.6

With the energy system components and financial parameters established, we develop a simulation model that integrates these factors into a comprehensive analysis. This model enables scenario testing and the evaluation of different configurations of wind–storage integration, optimizing the economic and technical feasibility of the renewable energy transition at Raglan.

#### 4. Design, Sizing, and Modeling of the Wind Energy and Storage System

A MATLAB-based simulation model was developed to evaluate the performance of the Raglan mine energy network following the integration of additional wind turbines and energy storage. This model enables the simulation of various operational scenarios by incorporating multiple input parameters, including

- Wind energy production;
- Electricity and heat generation based on generator operation;
- Diesel fuel consumption;
- Energy storage dynamics (charging and discharging cycles).

The model operates on an hourly time scale over an entire year, allowing for a detailed analysis of key performance indicators such as

- Renewable energy penetration rate;
- Wind energy curtailment losses;
- Diesel fuel savings;
- Greenhouse gas (GHG) emissions reduction;
- Economic performance metrics (including financial feasibility analysis).

The MATLAB-based dynamic model provides a crucial tool for predicting system behavior under various configurations, eliminating the need for physical testing. It enables the identification of optimal energy management strategies while ensuring grid stability and cost-effectiveness.

The simulation framework is structured into four interdependent sub-models, which operate in an iterative process to capture the complex interactions between energy production, storage, and demand, as shown in the flowchart in Figure 10.

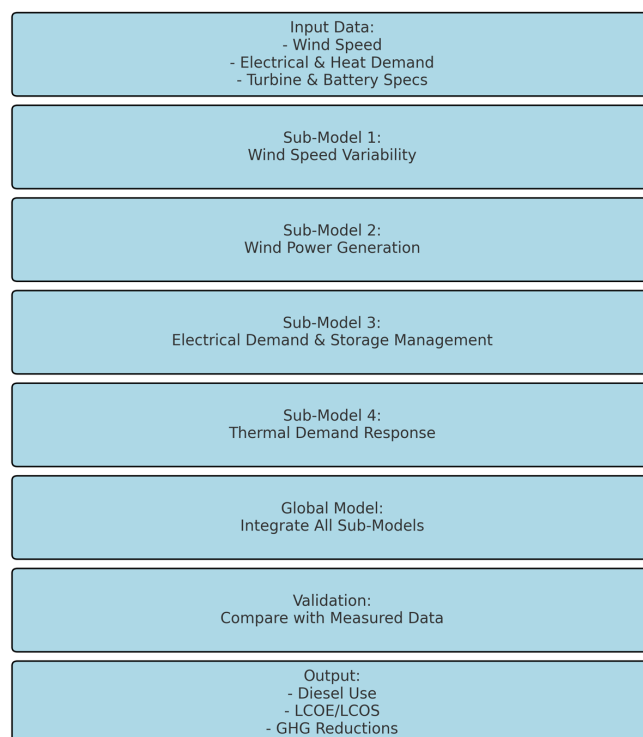


**Figure 10.** Modeling framework flowchart.

#### 4.1. Model Input Data

The MATLAB-based simulation program developed for this study is fully configurable, enabling flexible parameter adjustments tailored to specific simulation objectives. The operating parameters are structured within a “structure array” to enhance readability and clarity, facilitating efficient data organization and processing within the MATLAB workspace (see Figure 11). Key configurable parameters include

1x1 struct with 13 fields	
Field ▲	Value
Number of wind turbines	13
Wind power	4260
case	"favorable"
Raglan condition coefficient	0.8680
Number of generators	2
Average generator power	2.8739e+03
Exhaust gas Cp	1066
delta_t	228
Boiler consumption	10.6400
Maximum battery power	20000
Battery storage time	8
Max battery capacity	160000
Life time	15

**Figure 11.** Structure array of model input parameters.

- Number of wind turbines;
- Number of diesel generators in operation;
- Maximum battery power (maximum\_battery\_power);
- Battery storage duration (battery\_storage\_time);
- Total battery storage capacity (max\_battery\_capacity).

The structure array is linked to an internal MATLAB folder containing the essential datasets from the Raglan mining site, which are required for accurate simulation. These include

- Hourly heat demand data (2021);
- Wind speed data at 15 min intervals (2020);
- Electricity consumption data from the 25 kV network (hourly, 2020);
- The power curve of the ENERCON E-115 wind turbine.

By integrating these site-specific datasets, the MATLAB model enables a realistic and data-driven simulation, allowing for accurate assessments of wind energy integration, energy storage performance, and diesel displacement strategies at the Raglan mining site.

#### 4.2. Sub-Model 1: Wind Speed Model

This sub-model utilizes the “2020 Wind Data, 15 Minutes” dataset to simulate variations in wind speed under different conditions. For simulation purposes, three distinct wind scenarios were defined:

- Unfavorable: Wind speed decreases between  $-10\%$  and  $-5\%$ ;
- Random: Wind speed fluctuates within a range of  $-5\%$  to  $+5\%$ ;
- Favorable: Wind speed increases between  $+5\%$  and  $+10\%$ .

These conditions enhance the model’s flexibility, reflecting the natural variability of wind speeds, which fluctuate continuously. The simulation of wind speed variations is controlled by the following formula (Equation (1) and Equation (A4) in Appendix A):

$$r = a + (b - a) * rand(N, 1) \quad (1)$$

where

- $a$  and  $b$  are the lower and upper bounds of the wind speed variation interval;
- $N$  represents the random numbers within the interval  $(a, b)$ ;
- $rand(N, 1)$  is the MATLAB random function that generates values within the specified range.

A 15 min time step is used in the model, ensuring high-resolution variability in wind speed. Equation (1) serves as the MATLAB function for wind speed randomization, allowing for dynamic simulation of the 25 kV grid response, particularly regarding

- Wind turbine performance fluctuations;
- Energy storage system behavior under variable wind conditions;
- Grid stability under different wind penetration scenarios.

Additionally, this sub-model enables further analysis of critical wind conditions, such as

- The number of hours per year with no wind;
- Consecutive hours with zero wind generation;
- Consecutive hours without peak wind speeds.

By incorporating these stochastic wind variations, the model ensures a realistic assessment of wind energy intermittency and its impact on grid stability and energy storage requirements at the Raglan mining site.

#### 4.3. Sub-Model 2: Wind Power Generation Model

The wind power generation model is based on Sub-Model 1, utilizing the same 15 min time step for consistency. This sub-model incorporates the wind turbine's power curve (see Figure 7) and simulates energy production under varying wind conditions.

The model utilizes a MATLAB function, such as the 'SEARCHV' function in Microsoft Office, to accurately map wind speed values to corresponding power outputs, ensuring precise alignment between input wind speeds and turbine-generated power.

Given the harsh environmental conditions at Raglan (including cold temperatures, frost, and storms), a correction factor is applied to account for production inefficiencies. This factor was determined using real-world production data from the existing E-82 wind turbines, reflecting the actual site conditions. The correction factor is calculated as follows (Equation (2) and Equation (A8) in Appendix A):

$$\text{Corrective factor} = \frac{\text{Real production of the E-82 wind turbines}}{\text{Production obtained using its power curve from the supplier}} \quad (2)$$

Data analysis from 2019 to 2021 revealed that the E-82 wind turbines at Raglan produced only 86.8% of their theoretical capacity due to site-specific constraints. The same correction factor (0.868) was applied to the E-115 wind turbines to ensure realistic projections.

The time step is increased from 15 min to 1 h to facilitate further analysis, allowing for the following:

- Estimation of the wind farm's load factor;
- Calculation of total wind energy production (based on the number of new turbines installed);
- Computation of average hourly energy output per turbine.

Following multiple simulation iterations, the average load factor of the E-115 wind turbines was determined to be 43.6%. Subsequent calculations use this value to refine energy output estimations and assess the wind farm's overall performance under Raglan's environmental conditions.

#### 4.4. Sub-Model 3: Model of the Response to Electrical Demand

The electrical demand response model simulates the behavior of the 25 kV network under different load conditions. This sub-model is essential for monitoring and controlling:

- Battery management (state of charged and discharged energy);
- Unused surplus energy;
- Generator consumption.

To introduce flexibility, a randomization factor is applied to simulate variations in electrical demand. The model uses Equation (1) (previously introduced) with a random fluctuation range of −5% to +10%, ensuring a realistic simulation of demand changes.

A key objective of this sub-model is to ensure that the 25 kV network maintains a surplus of energy, enabling efficient battery storage and load management. Additionally, it anticipates future increases in electrical demand, given that the Raglan mine plans to expand nickel production.

Complete decarbonization is not immediately feasible since the ore-drying process relies entirely on diesel generators. Thus, the model accounts for the continued operation of some generators to meet heat demand, ensuring a pragmatic transition to renewable energy.

Two scenarios were tested to analyze the behavior of the 25 kV network under different supply and demand conditions:



1. Electricity demand is satisfied:
  - The energy supply exceeds demand, generating excess power.
  - The surplus is directed toward charging storage batteries.
  - If batteries are fully charged, the excess energy is curtailed (rejected).
  - This is the ideal case for the Raglan mine, as it maximizes the utilization of renewable energy.
2. Electricity demand is not satisfied:
  - The 25 kV network draws from battery storage to cover the deficit.
  - If battery reserves are insufficient, additional power must be generated.
  - In this case, an emergency recourse to diesel generators is triggered.
  - Each generator has an estimated power output of 2.88 MW.

Figure 12 illustrates Sub-Model 3's operating structure and details how energy demand, supply, and storage interact within the MATLAB simulation framework.

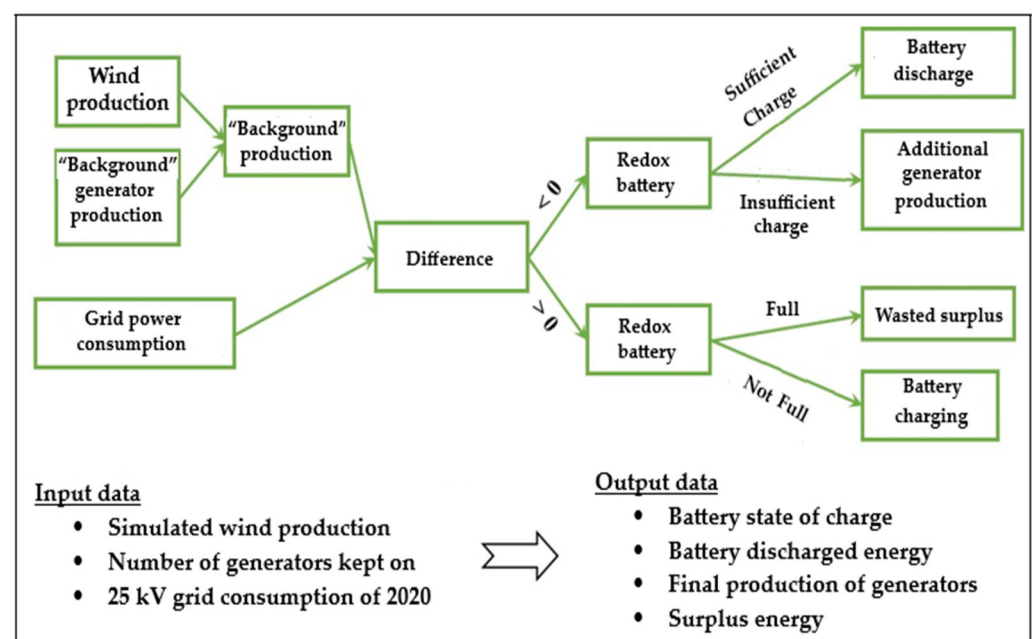


Figure 12. Management of the electrical part of the MATLAB model.

#### 4.5. Sub-Model 4: Thermal Demand Response Model

At the Raglan mine site, heat is generated through two primary sources:

- Heat recovery from EMD engine blocks;
- Diesel-fired boilers.

The thermal energy sub-model is based on operational data from 2021, during which 87% of the energy produced by diesel generators was recovered and utilized for heating through the cooling circuit—a particularly critical process during the cold months at Raglan.

The model integrates specific heat recovery values from two key sources:

- Exhaust gas recovery: 5.12 MWh;
- 31-HX-02 heat exchanger recovery: 12.35 MWh.

Additionally, the model predicts the contribution of wind energy to the heating circuit. When the diesel generator output is insufficient, surplus wind energy is directed to compensate for the heat demand.

Figure 13 illustrates a simplified schematic of the thermal management sub-model, depicting how different energy sources interact to maintain the site's heating requirements.

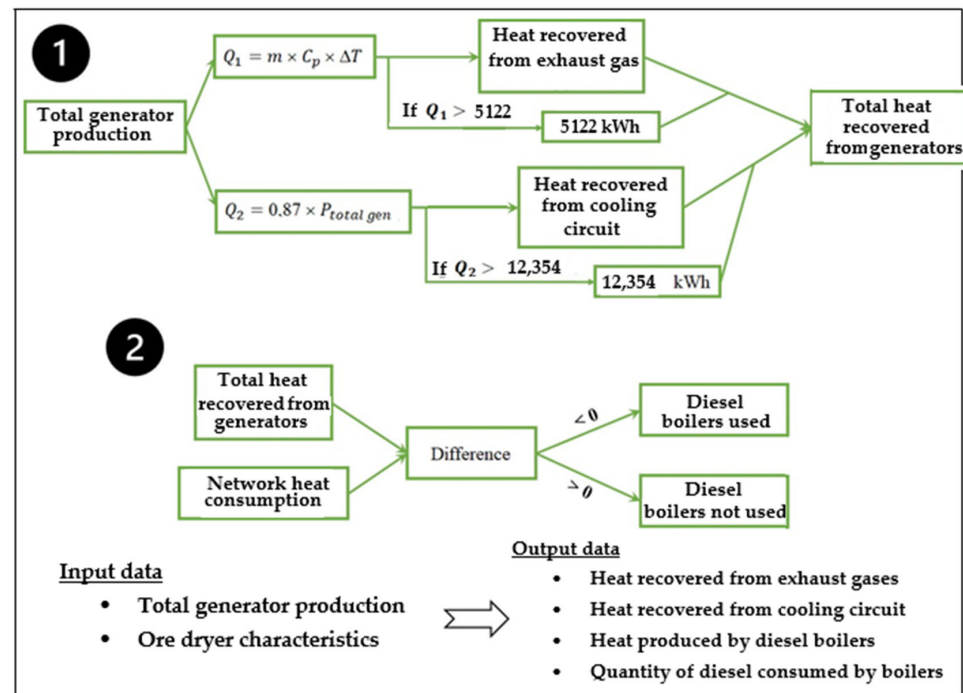


Figure 13. Thermal part management.

## 5. Validation of the Global Model

The global model integrates the four sub-models presented earlier, providing a comprehensive simulation of the Raglan energy system. This model accounts for both existing infrastructure and newly proposed installations, ensuring a realistic representation of energy production, storage, and consumption at the site.

To guarantee accuracy and computational efficiency, the MATLAB-based program has been thoroughly tested for

- Error-free execution;
- Optimized calculation times;
- Seamless operation with a single command.

The MATLAB simulation results are automatically exported to an Excel file using the “writetable” function to facilitate further analysis and generate structured data tables.

Its predictions were compared against actual operating data from the Raglan mining site to validate the model’s accuracy. The results are presented in Table 7.

Table 7. Comparison between actual plant data and the present work.

Characteristics	Modeled Value	Real Value	Relative Error (%)
Diesel consumed by generators (L)	37,979,558	37,141,356	2.26
Diesel consumed by boilers (L)	111,815	111,182	0.57
Total diesel consumed by the 25 kV network (L)	38,091,374	37,252,539	2.25
Wind power production (MWh)	16,286	16,871	3.59

The low relative errors observed in all key parameters confirm the accuracy and reliability of the simulation. The results demonstrate that the model provides a realistic approximation of the Raglan mine's energy system, making it a valuable tool for assessing new renewable energy integration and optimizing system performance.

## 6. Results and Discussion

### 6.1. Data

Table 8 presents the data and operating parameters used for modeling and simulation. These values are essential for sizing the wind farm's energy storage system and estimating the electricity and heat demand at the Raglan site.

**Table 8.** Model input and output data.

Data at the Entrance	Value
Exchange rate as of 21 September 2022	1.34 CAD/USD
Load factor (%)	32%
Lifetime of project (yr)	15.00
IRENA Canada Wind OPEX (CAD/kW.yr)	35.00
IRENA Canada Wind CAPEX (CAD/kW.yr)	1368
Exits	Value
CAPEX (CAD/MWh)	49.24
OPEX (CAD/MWh)	24.15
LCOE (CAD/MWh)	73.40

Several additional site-specific parameters were used in the modeling process:

- Wind speed at Raglan: Monthly average wind speed is typically between 6 and 9 m/s.
- The overall efficiency of electricity production by generators is 3.78 kWh/L, corresponding to an electricity generation efficiency of 35.5%.
- Air density: Approximately 1.37 kg/m<sup>3</sup>, based on an average atmospheric temperature of −15 °C, a common condition at Raglan.

The following assumptions were made regarding energy production and consumption data:

- Wind energy production data from 2020 was used as the baseline for modeling wind power generation.
- Electricity consumption data from 2020 was used to model the electrical demand of the mine.
- Thermal energy consumption data from 2021 was used to represent the mine's heating requirements.

By integrating these parameters and historical datasets, the model accurately represents the energy dynamics at the Raglan site, supporting the optimization of wind energy integration, energy storage, and system performance.

### 6.2. Model Results

This section presents the simulation results of the proposed model, which aims to decarbonize the Raglan mining site by integrating a vanadium flow battery storage system coupled with a wind farm.

The primary objective of this study is to develop optimized solutions that

- Reduce diesel consumption, lowering operational costs and reliance on fossil fuels;

- Decrease greenhouse gas (GHG) emissions, mitigating the environmental impact of mining activities.

The following subsections provide an in-depth analysis of the model's performance, including energy production, storage efficiency, and the potential for diesel displacement through the integration of renewable energy.

#### 6.2.1. General Trend Results

To significantly reduce diesel consumption, a large penetration of wind energy in the energy mix is necessary, which implies the installation of additional wind turbines. This is the only way to reduce diesel consumption and the number of installed generators. The different simulations focus on three main variables: the number of generators to be left running permanently throughout the year, which varies from zero to three; the battery capacity, which can take values of 0 MWh, 80 MWh, 120 MWh, and 160 MWh; and the additional number of E-115 wind turbines to be installed, which varies from 0 to 12.

Tables 9 and 10 provide a visual representation of the different configurations, enabling easy identification of diesel savings. It presents the diesel consumption reduction (as a percentage of diesel saved compared to the status quo) for the different configurations, considering all combinations of the number of new wind turbines, the battery capacity, and the number of generators to be kept running. Table 9 shows that significant diesel savings of up to 63.98% can be achieved. This is only possible by stopping all generators while increasing the number of wind turbines and the storage capacity of the flow battery.

**Table 9.** Amount of diesel saved, in the cases of 120 MWh and 160 MWh redox battery.

Number of Wind Turbines	160 MWh Redox Battery				120 MWh Redox Battery			
	0 gen	1 gen	2 gen	3 gen	0 gen	1 gen	2 gen	3 gen
12	−63.98%	−58.66%	−51.98%	−41.84%	−62.72%	−57.43%	−50.82%	−40.88%
11	−62.83%	−57.69%	−51.27%	−41.28%	−61.56%	−56.44%	−50.08%	−40.37%
10	−61.45%	−56.59%	−50.35%	−40.79%	−60.20%	−55.34%	−49.12%	−39.76%
9	−59.82%	−55.34%	−49.33%	−40.13%	−58.63%	−54.10%	−48.15%	−39.08%
8	−57.85%	−53.71%	−48.14%	−39.32%	−56.71%	−52.58%	−46.95%	−38.23%
7	−55.19%	−51.75%	−46.75%	−38.29%	−54.20%	−50.68%	−45.61%	−37.17%
6	−51.24%	−49.12%	−44.79%	−37.13%	−50.51%	−47.99%	−43.78%	−36.02%
5	−45.15%	−44.70%	−42.17%	−35.43%	−44.82%	−44.12%	−41.11%	−34.44%
4	−37.87%	−37.96%	−37.46%	−32.95%	−37.79%	−37.70%	−36.86%	−32.18%
3	−30.06%	−29.83%	−29.52%	−27.95%	−29.96%	−29.86%	−29.46%	−27.49%
2	−20.62%	−20.62%	−20.34%	−19.21%	−20.65%	−20.59%	−20.29%	−19.20%
1	−10.14%	−10.20%	−10.07%	−9.23%	−10.19%	−10.17%	−10.17%	−9.21%
0	0.73%	0.74%	0.61%	0.96%	0.71%	0.66%	0.68%	1.09%

Legend: Dark green = very good economy; Light green = good economy; Yellow = fairly good economy; Red = bad economy; gen = generator.

The reduction in diesel consumption is directly linked to the penetration of wind energy into the Raglan mine's energy mix; logically, the greater the number of wind turbines built, the more significant the proportion of wind energy in Raglan's energy mix. As a result, diesel consumption and the number of operating generators decrease. As such, the diesel savings increase by reducing the number of generators in operation, as well as by increasing battery capacity and wind turbine capacity. By leaving three generators in operation, we can achieve diesel savings of 35.44%, 39.66%, 40.88%, and 41.84% for the 0 MWh (without battery), 80 MWh, 120 MWh, and 160 MWh battery sizes. Besides this, the best diesel savings options, in the case of removing all generators and integrating 12 additional wind turbines into the grid, amount to 56.68%, 61.27%, 62.72%, and 63.98%, respectively, for the 0 MWh (without battery), 80 MWh (see Table 10), 120 MWh, and

160 MWh batteries (see Table 9). In contrast, with four wind turbines added to the grid and one generator in continuous operation, the configuration with the largest storage capacity (160 MWh battery) remains the best option, with an estimated diesel savings rate of 37.96%.

**Table 10.** Amount of diesel saved, in the cases of without redox battery and 80 MWh redox battery.

Number of Wind Turbines	80 MWh Redox Battery				Without Redox Battery			
	0 gen	1 gen	2 gen	3 gen	0 gen	1 gen	2 gen	3 gen
12	−61.27%	−56.06%	−49.49%	−39.66%	−56.68%	−51.31%	−44.79%	−35.44%
11	−60.10%	−55.05%	−48.74%	−39.16%	−55.43%	−50.34%	−43.93%	−34.76%
10	−58.79%	−53.93%	−47.82%	−38.49%	−54.17%	−49.16%	−43.00%	−34.10%
9	−57.22%	−52.62%	−46.75%	−37.79%	−52.51%	−47.80%	−41.88%	−33.29%
8	−55.29%	−51.14%	−45.56%	−36.92%	−50.60%	−46.15%	−40.63%	−32.23%
7	−52.92%	−49.33%	−44.11%	−35.91%	−48.45%	−44.40%	−39.07%	−31.19%
6	−49.56%	−46.73%	−42.33%	−34.69%	−45.82%	−42.09%	−37.31%	−29.84%
5	−44.39%	−43.23%	−39.96%	−33.20%	−42.28%	−39.37%	−35.05%	−28.21%
4	−37.69%	−37.37%	−36.13%	−30.95%	−37.01%	−35.46%	−32.12%	−26.10%
3	−29.94%	−29.72%	−29.21%	−26.90%	−29.62%	−29.14%	−27.56%	−23.15%
2	−20.61%	−20.52%	−20.23%	−19.08%	−20.51%	−20.27%	−19.61%	−17.86%
1	−10.14%	−10.08%	−10.09%	−9.19%	−10.14%	−10.04%	−9.71%	−8.76%
0	0.71%	0.63%	0.51%	1.11%	0.64%	0.66%	0.72%	1.32%

Legend: Dark green = very good economy; Light green = good economy; Yellow = fairly good economy; Red = bad economy; gen = generator.

#### Scenario of Two Generators in Operation and 120 MWh Battery: Impact of Adding Wind Turbines to the 25 kV-G Network

This scenario evaluates the performance of a hybrid system with two continuously operating diesel generators and a 120 MWh redox flow battery. The number of additional E-115 wind turbines varies from 0 to 12 to assess their impact on system costs and operation. The results are shown in Figure 14:

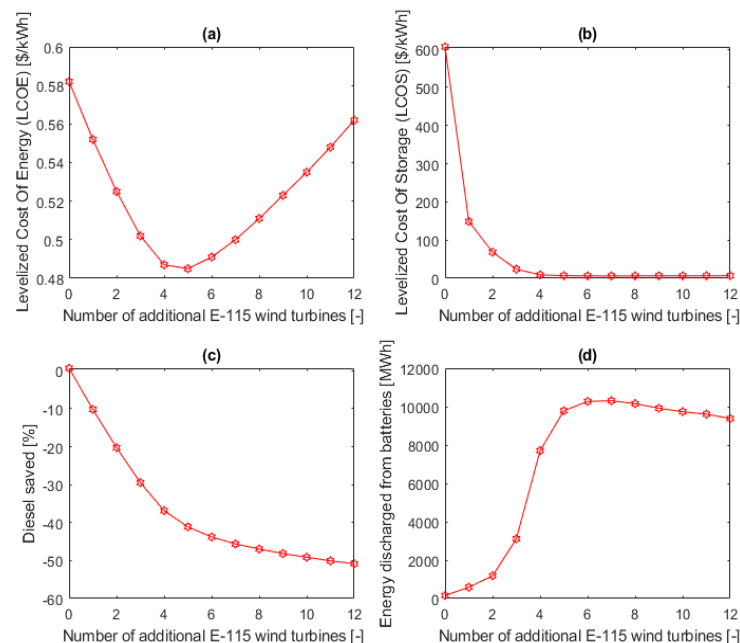


**Figure 14.** Performance indicator variation with the number of wind turbines (WTs) for a system with 120 MWh battery and two generators running continuously: (a) LCOE vs. number of WTs; (b) LCOS vs. number of WTs; (c) diesel savings vs. number of WTs; (d) energy discharged from batteries vs. number of WTs.



(a) Levelized Cost of Energy (LCOE): The LCOE initially decreases as wind turbines are added, reaching a minimum of around four turbines, beyond which further additions lead to a gradual increase. This reflects that the optimal integration point of wind energy before overcapacity leads to diminishing returns (see Equation (A1) in Appendix A).

(b) Levelized Cost of Storage (LCOS): LCOS sharply decreases with the addition of wind turbines and approaches zero after four turbines, indicating maximal economic utilization of the battery system beyond that point (see Equation (A2) in Appendix A).

(c) Diesel Savings: Increasing wind capacity consistently reduces diesel usage. However, the rate of diesel savings declines with each additional turbine, illustrating a saturation effect.

(d) Battery Discharge Energy: The energy discharged from the battery increases with added wind power, peaking at around six turbines. Beyond this point, battery usage stabilizes or slightly declines, suggesting that excess wind generation reduces reliance on storage.

This analysis highlights the trade-offs between wind capacity, storage utilization, and diesel consumption. An optimal configuration emerges with four to six additional turbines, effectively balancing cost and performance.

In addition to the analysis of the number of installed wind turbines, we explore the variation in the previous parameters with the wind penetration rate related to both installed capacity and the specific site operating conditions:

$$\text{Wind Penetration}(\%) = WP(\%) = \frac{E_{\text{wind}}}{E_{\text{load}}} \times 100 \quad (3)$$

As such, in Figure 15, we account for the actual wind energy contribution over a year, not just the installed capacity. Although the overall trends in Figure 15 resemble those in Figure 14, key distinctions emerge in subfigures (b) and (c):

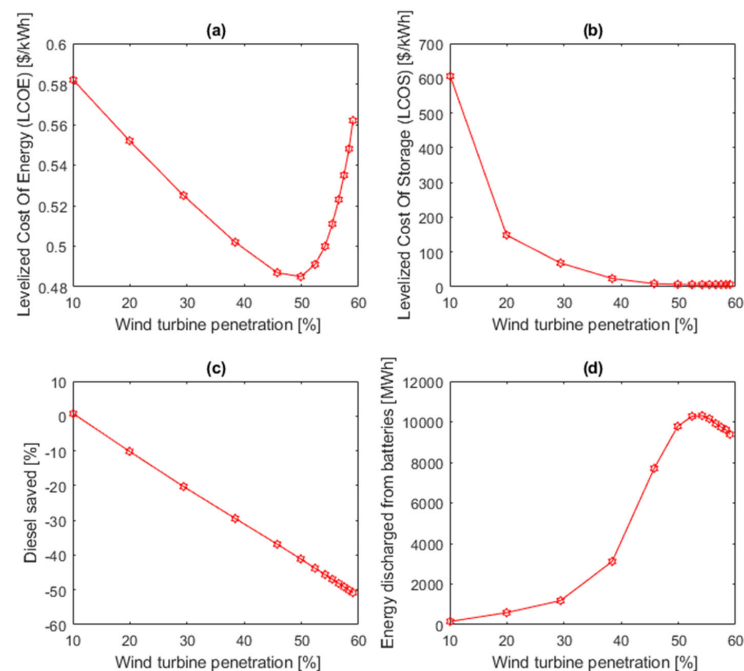


**Figure 15.** Performance indicator variation with the wind power penetration rate (WPP, %) for a system with 120 MWh battery and two generators running continuously: (a) LCOE vs. WPP; (b) LCOS vs. WPP; (c) diesel savings vs. WPP; (d) energy discharged from batteries vs. WPP.

(a) The Levelized Cost of Energy (LCOE) steadily decreases as wind penetration increases from 10% to 50%, reaching a minimum of approximately CAD 490/MWh at 50%. Beyond this point, the LCOE rises, indicating an optimal penetration level of around 50%.

(b) The Levelized Cost of Storage (LCOS) experiences a sharp decline between 10% and 20% wind penetration, after which the reduction becomes more gradual. LCOS reaches zero at 50% penetration, confirming this as the most economically efficient point for storage operation.

(c) Diesel consumption shows an almost linear decrease throughout the entire range of wind penetration, reinforcing a strong negative correlation between wind contribution and fossil fuel reliance.

(d) Battery discharge increases with wind penetration, peaking around 55% and then slightly decreasing. This suggests a saturation point in the contribution of storage to system balancing.

Together, these results confirm that a wind penetration rate of around 50% offers the best trade-off between cost reduction, storage utilization, and diesel offset in this configuration.

#### Impact of the Number of Operating Generators and Additional Wind Turbines on the Diesel Savings

For a system with a 120 MWh battery, Figure 16 illustrates the impact of wind turbine additions on diesel savings under different generator operation scenarios (0 to 3 generators running). The most significant diesel reduction occurs when no generators operate permanently, resulting in over 150% savings compared to the baseline. The >100% diesel savings reflect not only avoided electricity production from diesel but also the replacement of diesel used for thermal needs (e.g., building or process heating) through excess wind energy and heat recovery. This indicates net-negative diesel consumption relative to the baseline for electricity generation only when combined power and heat offset benefits are considered.

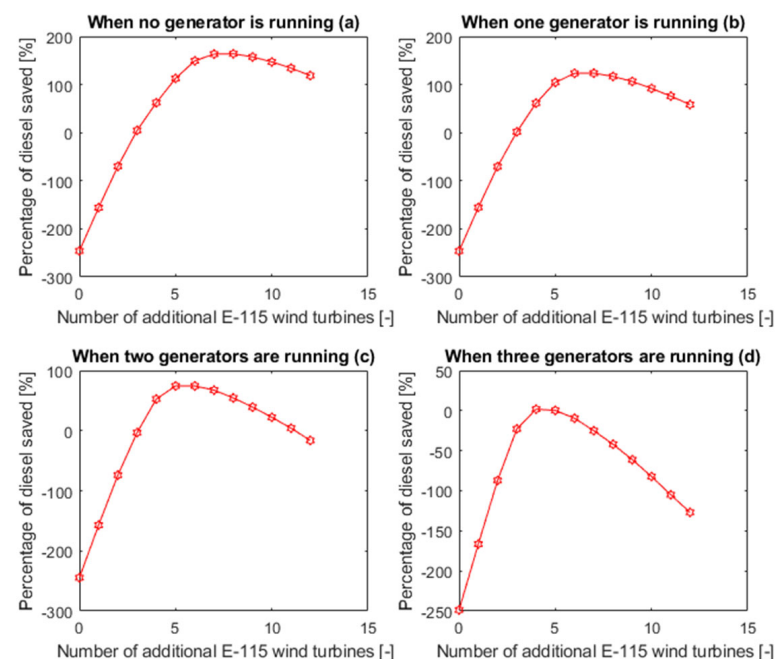


**Figure 16.** Share of diesel saved for different numbers of continuously running generators, depending on the number of wind turbines, with 160 MWh redox battery storage.

The relative diesel savings decrease as more generators remain permanently online (Figure 16b–d). This demonstrates that continuously operating diesel generation limits the economic and environmental benefits of wind integration.

#### 6.2.2. Results for the Most Economical Scenario

Economic performance is a primary driver for technology adoption in any industrial context, especially for mining operations. This section presents the results for the most cost-effective scenario over a 15-year project horizon.

As it is currently not feasible to fully disconnect all diesel generators due to ore processing and operational constraints, the most economical scenario involves maintaining two generators running continuously, integrating five E-115 wind turbines, and including a redox flow battery system rated at 20 MW/80 MWh. Under these conditions, the configuration with continuous operation of two generators outperforms the three-generator alternative in terms of both cost and environmental performance.

Table 11 presents the main characteristics of the most economical scenario. This scenario reduces 42,429.6 tCO<sub>2</sub> emissions, equivalent to 39.96% of the diesel consumed in Raglan annually. It also allows for savings of CAD 155.8 million. The return on investment is estimated at ten years.

**Table 11.** Results of the most economical scenario.

Data Type	Value	Unit
Wind CAPEX (5 wind turbines)	103.4	M CAD
CAPEX redox (battery and hangar)	149.5	M CAD
TOTAL CAPEX	253.0	M CAD
CAPEX additional cost	236.3	M CAD
TOTAL Economy	155.8	M CAD
LCOE complete system	460	CAD/MWh
LCOS complete system	7830	CAD/MWh
Wind integration	80.48	%
Wind penetration	48.71	%
Diesel saved	39.96	%
Quantity of GHG avoided	42,429	tCO <sub>2</sub> eq.

“CAPEX Additional Cost” refers to the incremental investment required to deploy the hybrid system—batteries, wind turbines, and supporting infrastructure—compared to a business-as-usual scenario (diesel-only operation). CAPEX is calculated using Equation (A7) in Appendix A. Equation (A6) allows for the estimation of OPEX.

The high LCOS (CAD 7831/MWh) results from including building infrastructure costs (~25% of total) and the high capital intensity of redox flow storage, especially in remote, harsh-climate environments like Raglan.

#### 6.2.3. Scenarios with the Highest Diesel Savings

As observed in Tables 9 and 10, the scenario with the highest diesel savings involves a large-scale hybrid configuration comprising a wind farm of 14 turbines, of which 12 are additional E-115 units, coupled with a 160 MWh redox flow battery. In its initial form, no diesel generators are running continuously. Under these conditions, the system achieves substantial environmental benefits, with an estimated reduction of 68,000 tCO<sub>2</sub> equivalent,

corresponding to a diesel savings rate of 63.98%. However, this scenario is infeasible at Raglan, primarily due to operational constraints related to ore drying.

Considering the actual operation conditions, the ore drying process at Raglan relies entirely on heat recovered from the exhaust gases of diesel engine blocks. Since the process requires continuous thermal input, a realistic scenario requires keeping two generators running in the implemented scenario. Thus, the finalized configuration includes 12 additional E-115 wind turbines, a 160 MWh redox flow battery system, and two diesel generators operating continuously. The technical and economic results for this high diesel-reduction scenario are summarized in Table 12. It is noted that the LCOE in the case of the most economical scenario is lower (Table 11), compared to that of the scenario with high diesel savings. This is explained by the fact that the total cost of energy production with high diesel savings uses a large share of energy from wind turbines, the production cost of which, at the Raglan site, is high, associated with this, the limited lifespan (15 years for wind turbines at Raglan, while the LCOE is often calculated for lifespans of 20 or 25 years) of renewable energy equipment (due to the cold climate, difficult maintenance). In the case of LCOS, the scenario with the greatest diesel savings presents a low value, i.e., CAD 6110/MWh (see Table 12).

**Table 12.** Results of the scenario with high diesel economy.

Data Type	Value	Unit
Wind CAPEX (12 wind turbines)	248.3	M CAD
CAPEX redox (battery and hangar)	253.6	M CAD
TOTAL CAPEX	501.9	M CAD
CAPEX additional cost	485.2	M CAD
TOTAL Economy	−16.3	M CAD
LCOE complete system	590	CAD/MWh
LCOS complete system	6110	CAD/MWh
Wind integration	45.81	%
Wind penetration	60.09	%
Diesel saved	51.98	%
Quantity of GHG avoided	55,203	tCO <sub>2</sub> eq.

### 6.3. Discussion

The results presented in this study are based on a model built with several conservative assumptions. Consequently, real-world outcomes may be even more favorable. For instance, actual wind power generation could exceed projections, battery utilization might be higher, diesel prices could rise, and the cost of redox flow technology may decrease over time.

One of the most significant cost drivers in the current analysis is the purchase and installation of redox flow batteries. As this technology has not yet reached full industrial maturity, large-scale systems like those required at Raglan remain rare and costly. Additionally, the need to construct a dedicated facility to house the tanks and electrochemical stacks adds substantial capital costs, unlike storage systems that do not require such infrastructure. Despite these limitations, most configurations analyzed yield a positive return on investment.

Soon, Raglan may be eligible for government subsidies to support decarbonization projects. If such funding is secured, it would reduce total project costs and significantly improve profitability. However, since the amount and timeline of potential subsidies remain uncertain, they have not been included in the current financial assessment.

Another potential but unquantified benefit is the commercial value of decarbonized or “green” nickel. Once Raglan completes its decarbonization process, it could position its nickel as a low-carbon product, an attractive feature for the growing electric vehicle (EV) industry. This could give Raglan a strategic commercial advantage in emerging clean technology markets.

The study also highlights that removing diesel generators from the 25 kV-G network is more effective in reducing emissions than simply increasing storage capacity. This aligns with Raglan’s plans for the second phase of its decarbonization strategy, which involves retiring the remaining EMD diesel generators. To enable this, an alternative ore-drying process must be identified that does not rely on engine exhaust heat.

Once diesel generators are fully phased out, wind energy penetration is expected to increase significantly. At that point, a new challenge will emerge: ensuring the quality and stability of electricity integrated into the network. This will likely require careful management of power electronics, grid-forming inverters, and control systems to maintain voltage and frequency standards in a diesel-free environment.

## 7. Conclusions and Perspectives

This study explores the decarbonization of the Raglan mining site by expanding its wind farm and integrating a redox flow battery energy storage system. To set the record straight, a brief comparison of different energy storage technologies is also presented and discussed.

In the first phase, we analyzed wind potential data at the Raglan site to assess the feasibility of installing additional wind turbines that could replace the site’s diesel generators, which currently meet its electrical needs. The second phase focused on identifying the technical requirements for sizing and implementing the storage system, particularly by analyzing the site’s electrical and thermal demand. These factors are essential to ensure optimal operation of the combined wind–battery system.

A hybrid simulation model, consisting of four sub-models, was developed using MATLAB and Excel. The model evaluated various scenarios, including

- \* Full or partial decommissioning of diesel generators;
- \* The number of additional E-115 wind turbines to be added;
- \* The ideal energy storage capacity of the redox flow battery.

Each scenario was assessed using two key economic indicators: the levelized cost of Energy (LCOE) and the Levelized Cost of Storage (LCOS). The results indicate that completely removing diesel generators is currently not feasible, primarily because some processes, such as ore drying, depend on the residual heat from diesel engines. Consequently, maintaining at least two generators in continuous operation is necessary.

The study also highlights the significant cost of implementing redox flow batteries under current market conditions. The LCOS, estimated at 7831 CAD/MWh, is high due to the price and infrastructure requirements of the storage system. As a result, battery utilization remains low, making the widespread integration of redox storage at Raglan technically possible but economically challenging under current conditions.

While this work demonstrates the techno-economic feasibility of integrating wind energy and redox storage for decarbonization, it does not address the grid stability or power quality issues, such as voltage fluctuations, frequency regulation, grid inertia, and stability during high renewable penetration. These aspects are crucial for ensuring reliable and safe operation, particularly in remote and weather-exposed environments such as Raglan. They will be investigated in future work using dynamic power system simulation tools.



Additionally, model results were compared with literature benchmarks for validation. While the current model is robust, further work is needed to refine the operating parameters and reduce reliance on assumptions. This will ensure more accurate and scalable projections for wind integration.

Future studies will focus on the following aspects:

- Detailed sensitivity and uncertainty analysis of key parameters (wind variability, energy demand, climate trends);
- Probabilistic modeling to assess long-term performance and reliability under varying environmental and operational conditions;
- Power system simulations to evaluate voltage and frequency stability under high-renewable-integration scenarios.

These next steps will provide a more comprehensive understanding of the technical and economic dynamics of large-scale decarbonization of remote industrial sites.

**Author Contributions:** Conceptualization, A.R. and D.R.R.; methodology, A.R., D.R.R., B.-J.R.M.B. and A.I.; software, A.R.; validation, D.R.R. and B.-J.R.M.B.; formal analysis, A.R., D.R.R., B.-J.R.M.B. and A.I.; investigation, A.R. and D.R.R.; resources, D.R.R.; data curation, A.R.; writing—original draft preparation, A.R., D.R.R. and B.-J.R.M.B.; writing—review and editing, D.R.R. and A.I.; visualization, A.R. and B.-J.R.M.B.; supervision, D.R.R.; project administration, D.R.R.; funding acquisition, D.R.R. All authors have read and agreed to the published version of the manuscript.

**Funding:** The authors thank Glencore and Hatch industrial partners for their support during this project. They also acknowledge the FRQ-NT's financial support via grants 322720, 340327, and 364164, as well as NSERC's grant RGPIN-2025-04831 and the Michel Trottier private donation to the T3E research group.

**Institutional Review Board Statement:** Not applicable.

**Informed Consent Statement:** Not applicable.

**Data Availability Statement:** The original contributions presented in this study are included in the article. Further inquiries can be directed to the corresponding author.

**Acknowledgments:** The authors acknowledge the data and information from the industrial partners Glencore and Hatch. The authors did not use generative AI technologies while preparing this work. The authors utilized AI-assisted technologies, including Grammarly ([www.grammarly.com](https://www.grammarly.com)) and Antidote ([www.antidote.info](https://www.antidote.info)), to enhance formulation and eliminate grammatical errors. After using this tool/service, the author(s) reviewed and edited the content as needed and take(s) full responsibility for the publication's content.

**Conflicts of Interest:** The authors declare no conflicts of interest.

## Appendix A

Table A1 gives a summary of the main equations used in this model.

**Table A1.** Main equations used in this model.

Equation	Equation Number	Variable	Observation	Meaning of Terms
$LCOE \left[ \frac{\$}{kWh} \right] = \frac{\sum_{t=1}^T \frac{CAPEX_t[\$] + OPEX_t[\$]}{(1+i(\%))^t}}{\sum_{t=1}^T \frac{Q_t[kWh]}{(1+i(\%))^t}}$	(A1)	LCOE	Equation taken from the IRENA [43] report “Renewable power generation costs 2021”	$CAPEX_t$ : investment expenditure for year $t$ $OPEX_t$ : operating and maintenance and fuel expenses during year $t$ $Q_t$ : electricity production during year $t$ $i$ : discount rate $T$ : system lifetime
$LCOS \left[ \frac{\$}{kWh} \right] = \frac{CAPEX_t[\$] + \sum_{t=1}^T \frac{OPEX_t[\$]}{(1+i(\%))^t} + \sum_{t=1}^T \frac{Charging\ cost[\$]}{(1+i(\%))^t} + \frac{End-of-life\ cost[\$]}{(1+i(\%))^{T+1}}}{\sum_{t=1}^T \frac{Elec\ discharged[kWh]}{(1+i(\%))^t}}$	(A2)	LCOS	The LCOS equation is taken from the work of Schmidt et al. [38].	$Charging\ cost$ : cost of electricity (or more broadly of energy) needed to power the system. $End - of - life\ cost$ : either the dismantling cost or the value of the installation at the end of the system’s life (salvage value) $Elec^{discharged}$ : annual amount of electricity discharged by the system
$Q = m \times Cp \times \Delta T$	(A3)	Amount of heat	The specific heat capacity of the exhaust gases is taken as 1066 J/kg.K	$m$ : mass $Cp$ : The specific heat capacity of the exhaust gases $\Delta T$ : Temperature variation
$r = a + (b - a) * rand(N, 1)$	(A4)	Wind speed	The simulation of wind speed variations	$a$ and $b$ are the lower and upper bounds of the wind speed variation interval $N$ represents the random numbers within the interval $(a, b)$ $rand(N, 1)$ is the MATLAB random function that generates values within the specified range.
$f_{\lambda}(x; \lambda, k) = \begin{cases} \frac{k}{\lambda} \left(\frac{x}{\lambda}\right)^{k-1} e^{-\left(\frac{x}{\lambda}\right)^k}; & \text{if } x \geq 0 \\ 0 & ; \text{if } x < 0 \end{cases}$	(A5)	The Weibull distribution	The Weibull distribution is used to estimate the annual mean wind speed at Raglan.	$\lambda$ the scale factor, $k$ the shape factor and; $x$ the wind speed.
$OPEX \left[ \frac{\$}{MWh} \right] = \frac{1000}{Fc \times 8760} \times OPEX \left[ \frac{\$}{kWh} \right]$	(A6)	OPEX	LCOE corresponds to the addition of CAPEX and OPEX.	$Fc$ : load factor
$CAPEX \left[ \frac{\$}{MWh} \right] = \frac{1000}{Fc \times 8760 \times D} \times CAPEX \left[ \frac{\$}{kW} \right]$	(A7)	CAPEX	LCOE corresponds to the addition of CAPEX and OPEX.	$Fc$ : load factor $D$ : project lifespan
$Corrective\ factor = \frac{Real\ production\ of\ E-82\ wind\ turbines}{production\ obtained\ using\ its\ power\ curve\ from\ the\ supplier}$	(A8)	correction factor		The correction factor is applied to account for production inefficiencies. It takes into account the harsh environmental conditions in Raglan (cold, frost, storms, etc.).

## References

- United Nations. Framework convention on climate change. In Proceedings of the Report of the Conference of the Parties on Its Twenty-First Session, Paris, France, 30 November–11 December 2015; Part One: Proceedings. p. 42.
- Jahangiri, Z.; Hendriks, R.; McPherson, M. A Machine Learning Approach to Analysis of Canadian Provincial Power System Decarbonization. *Energy Rep.* **2024**, *11*, 4849–4861. [\[CrossRef\]](#)
- Government of Canada. Canada's Official Greenhouse gas Inventory. *Annex 13—Electricity in Canada*. Available online: <https://open.canada.ca/data/en/dataset/779c7bcf-4982-47eb-af1b-a33618a05e5b> (accessed on 9 January 2025).
- Government of Canada. Canadian Net-Zero Emissions Accountability Act. Available online: <https://www.canada.ca/en/services/environment/weather/climatechange/climate-plan/net-zero-emissions-2050/canadian-net-zero-emissions-accountability-act.html> (accessed on 9 January 2025).
- Saffari, M.; McPherson, M. Assessment of Canada's Electricity System Potential for Variable Renewable Energy Integration. *Energy* **2022**, *250*, 123757. [\[CrossRef\]](#)
- Nielsen, A.S.; Del Alamo Serrano, G.; Schanche, T.L.; Burheim, O.S. Reducing CO<sub>2</sub> Emissions, Energy Consumption, and Decarbonization Costs in Manganese Production by Integrating Fuel-Assisted Solid Oxide Electrolysis Cells in Two-Stage Oxide Reduction. *Appl. Energy* **2025**, *377*, 124572. [\[CrossRef\]](#)
- Da Silva, F.T.F.; Garcez Lopes, M.S.; Asano, L.M.; Angelkorte, G.; Brambilla Costa, A.K.; Szklo, A.; Schaeffer, R.; Coutinho, P. Integrated Systems for the Production of Food, Energy and Materials as a Sustainable Strategy for Decarbonization and Land Use: The Case of Sugarcane in Brazil. *Biomass Bioenergy* **2024**, *190*, 107387. [\[CrossRef\]](#)
- Du, Y.; Shen, X.; Kammen, D.M.; Hong, C.; Nie, J.; Zheng, B.; Yao, S. A Generation and Transmission Expansion Planning Model for the Electricity Market with Decarbonization Policies. *Adv. Appl. Energy* **2024**, *13*, 100162. [\[CrossRef\]](#)
- Balaban, G.; Dumbrava, V.; Lazaroiu, A.C.; Kalogirou, S. Analysis of Urban Network Operation in Presence of Renewable Sources for Decarbonization of Energy System. *Renew. Energy* **2024**, *230*, 120870. [\[CrossRef\]](#)
- Dongsheng, C.; Ndifor, E.Z.; Temidayo Olayinka, A.-O.; Ukwuoma, C.C.; Shefik, A.; Hu, Y.; Bamisile, O.; Dagbasi, M.; Uzun Ozsahin, D.; Adun, H. An EnergyPlan Analysis of Electricity Decarbonization in the CEMAC Region. *Energy Strategy Rev.* **2024**, *56*, 101548. [\[CrossRef\]](#)
- Obiora, S.C.; Bamisile, O.; Hu, Y.; Ozsahin, D.U.; Adun, H. Assessing the Decarbonization of Electricity Generation in Major Emitting Countries by 2030 and 2050: Transition to a High Share Renewable Energy Mix. *Heliyon* **2024**, *10*, e28770. [\[CrossRef\]](#)
- Roshan Kumar, T.; Beiron, J.; Marthala, V.R.R.; Pettersson, L.; Harvey, S.; Thunman, H. Combining Exergy-Pinch and Techno-Economic Analyses for Identifying Feasible Decarbonization Opportunities in Carbon-Intensive Process Industry: Case Study of a Propylene Production Technology. *Energy Convers. Manag. X* **2025**, *25*, 100853. [\[CrossRef\]](#)
- Asri, L.I.M.; Ariffin, W.N.S.F.W.; Zain, A.S.M.; Nordin, J.; Saad, N.S. Comparative Study of Energy Storage Systems (ESSs). *J. Phys. Conf. Ser.* **2021**, *1962*, 012035. [\[CrossRef\]](#)
- Mahadevan, V.; S, S.R.; Rusho, M.A.; Yishak, S. Critical Review of Energy Storage Systems: A Comparative Assessment of Mechanisms, Advantages, Challenges, and Integration with Renewable Energy. *Results Eng.* **2025**, *26*, 105589. [\[CrossRef\]](#)
- Babaharra, O.; Choukairy, K.; Faraji, H.; Khallaki, K.; Hamdaoui, S.; Bahammou, Y. Thermal Performance Analysis of Hollow Bricks Integrated Phase Change Materials for Various Climate Zones. *Heat Transf.* **2024**, *53*, 2148–2172. [\[CrossRef\]](#)
- Liu, X.; Pan, L.; Rao, H.; Wang, Y. A Review of Transport Properties of Electrolytes in Redox Flow Batteries. *Future Batter.* **2025**, *5*, 100019. [\[CrossRef\]](#)
- Thamizhselvan, R.; Naresh, R.; Ulaganathan, M.; Pol, V.G.; Ragupathy, P. Achieving Exceptional Cell Voltage (2.34 V) through Tailoring pH of Aqueous Zn-Br<sub>2</sub> Redox Flow Battery for Potential Large-Scale Energy Storage. *Electrochim. Acta* **2023**, *441*, 141799. [\[CrossRef\]](#)
- Chen, H.; Zhang, X.; Zhang, S.; Wu, S.; Chen, F.; Xu, J. A Comparative Study of Iron-Vanadium and All-Vanadium Flow Battery for Large Scale Energy Storage. *Chem. Eng. J.* **2022**, *429*, 132403. [\[CrossRef\]](#)
- Sun, J.; Wu, M.; Jiang, H.; Fan, X.; Zhao, T. Advances in the Design and Fabrication of High-Performance Flow Battery Electrodes for Renewable Energy Storage. *Adv. Appl. Energy* **2021**, *2*, 100016. [\[CrossRef\]](#)
- Standard 34-2010; Designation and Safety Classification of Refrigerants. ANSI/ASHRAE: Atlanta, GA, USA, 2011.
- Huang, Z.; Mu, A.; Wu, L.; Wang, H.; Zhang, Y. Electrolyte Flow Optimization and Performance Metrics Analysis of Vanadium Redox Flow Battery for Large-Scale Stationary Energy Storage. *Int. J. Hydrog. Energy* **2021**, *46*, 31952–31962. [\[CrossRef\]](#)
- Loktionov, P.; Pichugov, R.; Konev, D. Neutralization Flow Batteries in Energy Harvesting and Storage. *J. Energy Storage* **2023**, *72*, 108467. [\[CrossRef\]](#)
- Ren, J.; Li, Y.; Wang, Z.; Sun, J.; Yue, Q.; Fan, X.; Zhao, T. Thermal Issues of Vanadium Redox Flow Batteries. *Int. J. Heat Mass Transf.* **2023**, *203*, 123818. [\[CrossRef\]](#)
- Zeng, D.; Mao, T.; Zhang, Z.; Dai, J.; Ouyang, J.; Xie, Z. A High-Performance Aqueous Eu/Ce Redox Flow Battery for Large-Scale Energy Storage Application. *Int. J. Heat Mass Transf.* **2024**, *233*, 125978. [\[CrossRef\]](#)

25. Ouyang, T.; Zhang, M.; Qin, P.; Tan, X. Flow Battery Energy Storage System for Microgrid Peak Shaving Based on Predictive Control Algorithm. *Appl. Energy* **2024**, *356*, 122448. [CrossRef]
26. Darling, R.M. Techno-Economic Analyses of Several Redox Flow Batteries Using Levelized Cost of Energy Storage. *Curr. Opin. Chem. Eng.* **2022**, *37*, 100855. [CrossRef]
27. Lourenssen, K.; Williams, J.; Ahmadpour, F.; Clemmer, R.; Tasnim, S. Vanadium Redox Flow Batteries: A Comprehensive Review. *J. Energy Storage* **2019**, *25*, 100844. [CrossRef]
28. CEA. RMN: Tout Savoir sur L'électrolyte Organique D'une Batterie à Flux Redox. Available online: <https://www.cea.fr/drf/Pages/Actualites/En-direct-des-labos/2023/rmn--tout-savoir-sur-lelectrolyte-organique-dune-batterie-a-flux-redox.aspx#:~:text=Les%20batteries%20%C3%A0%20flux%20redox,de%20stocker%20des%20charges%20%C3%A9lectriques> (accessed on 21 January 2025).
29. Zheng, N.; Wang, Q.; Ding, X.; Zhang, H.; Duan, L.; Wang, X.; Zhou, Y.; Sun, M.; Desideri, U. Techno-Economic Analysis of a Novel Solar-Based Polygeneration System Integrated with Vanadium Redox Flow Battery and Thermal Energy Storage Considering Robust Source-Load Response. *Appl. Energy* **2024**, *376*, 124288. [CrossRef]
30. Yesilyurt, M.S.; Ozcan, H.G.; Yavasoglu, H.A. Co-Simulation-Based Conventional Exergy Evaluation of a Hybrid Energy Generation-Vanadium Redox Flow Battery-Air Source Heat Pump System. *Energy* **2023**, *281*, 128301. [CrossRef]
31. Oshnoei, S.; Oshnoei, A.; Mosallanejad, A.; Haghjoo, F. Novel Load Frequency Control Scheme for an Interconnected Two-Area Power System Including Wind Turbine Generation and Redox Flow Battery. *Int. J. Electr. Power Energy Syst.* **2021**, *130*, 107033. [CrossRef]
32. Reynard, D.; Girault, H. Combined Hydrogen Production and Electricity Storage Using a Vanadium-Manganese Redox Dual-Flow Battery. *Cell Rep. Phys. Sci.* **2021**, *2*, 100556. [CrossRef]
33. Huang, Z.; Mu, A.; Wu, L.; Wang, H. Vanadium Redox Flow Batteries: Flow Field Design and Flow Rate Optimization. *J. Energy Storage* **2022**, *45*, 103526. [CrossRef]
34. Ulaganathan, M.; Aravindan, V.; Yan, Q.; Madhavi, S.; Skyllas-Kazacos, M.; Lim, T.M. Recent Advancements in All-Vanadium Redox Flow Batteries. *Adv. Mater. Interfaces* **2016**, *3*, 1500309. [CrossRef]
35. Hosseiny, S.S.; Wessling, M. Ion Exchange Membranes for Vanadium Redox Flow Batteries. In *Advanced Membrane Science and Technology for Sustainable Energy and Environmental Applications*; Elsevier: Amsterdam, The Netherlands, 2011; pp. 413–434. ISBN 978-1-84569-969-7.
36. Skyllas-Kazacos, M.; Menictas, C.; Lim, T. Redox Flow Batteries for Medium—to Large-Scale Energy Storage. In *Electricity Transmission, Distribution and Storage Systems*; Elsevier: Amsterdam, The Netherlands, 2013; pp. 398–441. ISBN 978-1-84569-784-6.
37. Emrani, A.; Achour, Y.; Sanjari, M.J.; Berrada, A. Adaptive Energy Management Strategy for Optimal Integration of Wind/PV System with Hybrid Gravity/Battery Energy Storage Using Forecast Models. *J. Energy Storage* **2024**, *96*, 112613. [CrossRef]
38. Cremoncini, D.; Di Lorenzo, G.; Frate, G.F.; Bischi, A.; Baccioli, A.; Ferrari, L. Techno-Economic Analysis of Aqueous Organic Redox Flow Batteries: Stochastic Investigation of Capital Cost and Levelized Cost of Storage. *Appl. Energy* **2024**, *360*, 122738. [CrossRef]
39. IRENA. *Electricity Storage and Renewables: Costs and Markets to 2030*; International Renewable Energy Agency: Abu Dhabi, United Arab Emirates, 2017; p. 132.
40. Schmidt, O.; Melchior, S.; Hawkes, A.; Staffell, I. Projecting the Future Levelized Cost of Electricity Storage Technologies. *Joule* **2019**, *3*, 81–100. [CrossRef]
41. Minke, C.; Turek, T. Materials, System Designs and Modelling Approaches in Techno-Economic Assessment of All-Vanadium Redox Flow Batteries—A Review. *J. Power Sources* **2018**, *376*, 66–81. [CrossRef]
42. Zheng, M.; Sun, J.; Meinrenken, C.J.; Wang, T. Pathways Toward Enhanced Techno-Economic Performance of Flow Battery Systems in Energy System Applications. *J. Electrochem. Energy Convers. Storage* **2019**, *16*, 021001. [CrossRef]
43. Zhang, M.; Moore, M.; Watson, J.S.; Zawodzinski, T.A.; Counce, R.M. Capital Cost Sensitivity Analysis of an All-Vanadium Redox-Flow Battery. *J. Electrochem. Soc.* **2012**, *159*, A1183–A1188. [CrossRef]
44. Noack, J.; Wietschel, L.; Roznyatovskaya, N.; Pinkwart, K.; Tübke, J. Techno-Economic Modeling and Analysis of Redox Flow Battery Systems. *Energies* **2016**, *9*, 627. [CrossRef]
45. Viswanathan, V.; Crawford, A.; Stephenson, D.; Kim, S.; Wang, W.; Li, B.; Coffey, G.; Thomsen, E.; Graff, G.; Balducci, P.; et al. Cost and Performance Model for Redox Flow Batteries. *J. Power Sources* **2014**, *247*, 1040–1051. [CrossRef]
46. IRENA. *Renewable Power Generation Costs in 2021*; International Renewable Energy Agency: Abu Dhabi, The Emirates, 2022; p. 204.
47. Tardy, A.; Rousse, D.R.; Mungyeke Bisulandu, B.-J.R.; Ilinca, A. Enhancing Energy Sustainability in Remote Mining Operations Through Wind and Pumped-Hydro Storage; Application to Raglan Mine, Canada. *Energies* **2025**, *18*, 2184. [CrossRef]
48. Durand, S.; Turcotte, P.; Haillet, D.; Rousse, D.R.; Arasteh, H.; Kalivogui, S.; Zhang, K.; Izquierdo, R.; Merabtine, A.; Maref, W.; et al. Decarbonization Strategies for Northern Canada: A Review of Renewable Energy and Energy Storage in off-Grid Communities. *Energy Convers. Manag. X* **2025**, *27*, 101055. [CrossRef]

49. VRB Energy. VRB Energy Announces UL1973 Certification for 1MW VRB-ESS. Available online: <https://vrbenergy.com/vrb-energy-announces-ul1973-certification-for-1mw-vrb-ess/> (accessed on 12 June 2025).
50. Stehly, T.; Duffy, P. *2020 Cost of Wind Energy Review*; Renewable Energy: Golden, CO, USA, 2022; p. 77.
51. Solar Huawei. Coût du Stockage D'énergie Solaire: Guide Pour les Propriétaires. Available online: <https://solar.huawei.com/tn/blog/tn/2024/solar-energy-storage-cost> (accessed on 22 January 2025).

**Disclaimer/Publisher's Note:** The statements, opinions and data contained in all publications are solely those of the individual author(s) and contributor(s) and not of MDPI and/or the editor(s). MDPI and/or the editor(s) disclaim responsibility for any injury to people or property resulting from any ideas, methods, instructions or products referred to in the content.